Structural and diagenetic signatures of a very shallow sub-volcanic intrusion into a carbonate platform (Albian, Basque-Cantabrian Basin, Northern Spain).

Ophélie Pascault, Christophe Durlet, Pierre-Alexandre Teboul, Maxime Ducoux, Jean-Pierre Girard, Aurélien Virgone, Thomas Saucède

Structural and diagenetic signatures of a very shallow sub-volcanic intrusion into a carbonate platform (Albian, Basque-Cantabrian Basin, Northern Spain).

Authors: Ophélie Pascault[1,2], Christophe Durlet[1], Pierre-Alexandre Teboul[3], Maxime Ducoux[4], Jean-Pierre Girard[3,5], Aurélien Virgone[3] and Thomas Saucède[1].

Affiliations

[1] Biogéosciences, UMR 6282 CNRS, Université de Bourgogne, 6 Boulevard Gabriel, 21000 Dijon, France.

[2]Akkodis, 4 rue Jules Ferry, 64000 Pau, France

[3]TotalEnergies, OneTech, CSTJF, avenue Larribau, 64000 Pau, France

[4] M&U SAS, 6 rue de Chamechaude, 38360 Sassenage, France

[5] Université de Pau et des Pays de l'Adour (UPPA), 64000 Pau, France

DOI: https://doi.org/10.1016/j.marpetgeo.2023.106175

Received Date: 24 October 2022; Revised Date: 6 February 2023; Accepted Date: 8 February 2023

Corresponding author: ophelie.pascault@akkodis.com

Full postal address: Ophélie Pascault - Akkodis, 4 rue Jules Ferry, Pau, France

Co-authors e-mail address:

christophe.durlet@u-bourgogne.fr

pierre-alexandre.teboul@totalenergies.com

maxime@mandu-geology.fr

girard.jean-pierre@univ-pau.fr

aurelien.virgone@totalenergies.com

thomas.saucede@u-bourgogne.fr

Highlights

- For the first time, early diagenetic signature of a very shallow sub-volcanic intrusion in carbonate platform is reported.
- The igneous body investigated in this paper intrudes an Urgonian carbonate platform of the Early Albian.
- The intrusion is located along a synsedimentary fault of the hyper-extended Basque-Cantabrian Basin.
- Structural, early diagenetic and geochemical data indicates an intrusion emplacement just below the paleo-seafloor (~50m).
- Pre- & post-intrusive hydrothermal circulations affecting early cements and specific facies related to seeps are reported.

Abstract

In several tectonic contexts and especially in hyper-extensive basins, magmatic rise may crosscut shallow marine carbonate series, forming either volcanic systems or only igneous intrusions at various depths. Impacts of these magmatic events on the surrounding carbonate sediments can be significant and are relatively well documented from a geometrical, sedimentological and hydrochemical point of view. Their diagenetic signature (e.g., early diagenetic phases in cases where magma reaches or approaches the surface) still remains poorly investigated. In this paper the authors use a multi-proxy approach combining morpho-structural, diagenetic (cement stratigraphy), geochemical (carbon and oxygen isotope, U-Pb dating) and sedimentological study to investigate the Larrano igneous body contemporaneous with the Urgonian limestones (Early Albian) of the Duranguesado platform, in the well-preserved and hyper-extended Basque-Cantabrian Basin. This investigative work produced several results: the first result, combining morpho-structural and sedimentological data, is the model of a basaltic magma rising along normal faults but stopping about fifty meters below the paleo-seafloor; another is the detailed description the "Larrano eogenetic anomaly" that includes cataclastic fractures, dissolution, Fe oxy-hydroxides, ferroan saddle dolomite and magnesian calcite. Such phases form an early diagenetic overprint around the igneous body and testify to the thermal shock and warm seawater circulation occurring at the time of and just after the intrusion. Pre-intrusive and post-intrusive hydrothermally-influenced cements and facies are also recorded and are perfectly calibrated by a detailed cement stratigraphy associated with a layering model of the sedimentary units. The role of magmatic CO_2 contribution is not quantified in the present study. Furthermore, the $\delta^{13}C$ signature of various cements, micrites and bioclasts suggests no thermogenic methane contribution, unlike other Albian magmatic intrusions hosted by different lithologies and recorded at various depths below the paleo-seafloor.

Keywords

Carbonate diagenesis; Volcanic intrusion; Saddle dolomite; Hydrothermal system; Urgonian carbonate platform; Albian; Basque-Cantabrian Basin.

1 Introduction

Hyper-extended basins are the seat of important geothermal anomalies and prone to magmatic injections within the sedimentary pile that commonly occur along or near major synsedimentary faults, leading to various cases of intrusive or effusive igneous bodies (Breitkreuz & Rocchi., 2018; Acocella, 2021; Ducoux et al., 2021; Lokier et al., 2021). Volcanic events directly in contact with ancient or recent carbonate platforms are well-documented (e.g., synthesis by Lokier, 2021). Notable examples are: (1) basaltic flows overlying platform sediments and inducing many changes in sedimentary environments e.g., temperature anomalies, chemical element input, new geomorphological structures (Carracedo-Sanchez et al., 2012; Baarli et al., 2014); (2) Volcanic breccias in which volcanic fragments are mixed together with carbonate clasts lying near eruptive structures (Castañares, et al., 1997; Martin et al., 2004; Basile & Chauvet, 2009; Courgeon et al., 2017); (3) Volcanic ash or clasts from distant eruptive center interstratified with platform carbonates (Robador & Garcia de Cortazar, 1986; Fernández-Mendiola & García-Mondéjar, 1995). In the latter example there is uncertainty as to the spatial relationship between the eruptive center and the platform. In contrast, documented cases of sub-volcanic intrusions (e.g., approaching but not reaching the surface) located right below neritic carbonates remain rare.

Studying the impact of sub-volcanic intrusions on carbonate environments and early diagenesis remains complicated due to difficulties in accurately dating such magmatic events. This is particularly true when intrusions are identified only on seismic sections, and not drilled

or sampled, or when core samples are available but are too deeply altered for direct dating with K-Ar or Ar-Ar radiometric methods for instance (Magee et al., 2015; Glazner et al., 2018; Planke et al., 2018). With sub-volcanic intrusions near the surface, indirect dating methods can be used by:

- Detection of interstratified sedimentary breccias, even if they are devoid of igneous particles, with typical characteristics of phreato-magmatic eruptions (Martin et al., 2004; Svensen et al, 2015; Agirrezabala et al, 2017).

- Identification of sealed synsedimentary forced folds and faults, a few decametres to a few hectometres above the intrusions. These can be detected in outcrops (Molina & Vera, 2000; Agirrezabala, 2015), or on seismic sections (Rui et al., 2013; Magee et al., 2014; Planke et al., 2018; Bischoff et al., 2021).

- Discovery of vent structures with specific interstratified facies (e.g., ores bodies, hydrothermally-influenced communities) located above the igneous intrusion (Mounji et al., 1988; Planke et al., 2005; 2018; Agirrezabala, 2009; Agirrezabala et al., 2013). In this case, the indirect dating method can be ambiguous, either because demonstrates the hypogean origin of a bedding-unconformable sedimentary body is difficult on seismic sections (Moller Hansen & Cartwright, 2006; Cartwright & Santamarina, 2015), or because the hydrothermal activity may have occurred before or after the igneous event itself (Belka, 1998; Jakubowicz et al., 2015).

- Determination of atypical early (very shallow) diagenesis in the surrounding rocks, chronologically and spatially linked to the igneous body (García-Garmilla & Carracedo-Sánchez, 1989; Shah et al., 2021). When intrusions are emplaced in a sedimentary sequence the surrounding rocks are impacted by: i) magmatically-induced local heating (i.e., contact metamorphism - Aarnes et al., 2011; Planke et al., 2018); ii) cataclastic or

hydraulic fractures with sedimentary injections; iii) hydrothermal diagenesis including dissolution, recrystallizations and cementations (Fe-rich minerals, dolomitization) developing during and after the intrusive event (Girard, 1985; Girard et al., 1989; Agirrezabala, 2009; Shah et al., 2021). Particular eogenetic textures and mineralogical signatures recording the influence of sub-volcanic intrusions are mostly documented in sandstones and shales (García-Garmilla & Carracedo-Sánchez, 1989; Agirrezabala, 2009; Magee et al., 2013) but remain poorly represented in shallow marine carbonate platforms.

The well-preserved hyper-extended Basque-Cantabrian Basin which developed during the Aptian-Albian records several cases of intrusive and volcanic igneous bodies crosscutting neritic sediments of the Urgonian platform. One of these bodies, previously interpreted as an example of intraplatform effusive basaltic event into the platform of Duranguesado (Fernández-Mendiola & García-Mondéjar 2003), is used in this paper as a reference case to study the sedimentary and diagenetic impact of such magmatic injections into shallow marine carbonate environments.

Using a complete morpho-structural and diagenetic approach (cement stratigraphy, geochemistry, U-Pb dating), combining previous sedimentological data from Fernández-Mendiola & García-Mondéjar (2003) with our own, enables us to present an integrated study.

The aims of the present study were twofold: (1) to demonstrate the value of coupling sedimentological, structural, and diagenetic studies, to specify the age and depth of the magmatic event moreover to characterize an early diagenetic signature as a consequence of magmatic injection emplacement; (2) to refine a scenario for the Larrano magmatic event and compare structural and early diagenetic signatures of the Larrano igneous event with other Albian magmatic episodes present in the Basque-Cantabrian Basin (Agirrezabala, 2009, 2015;

Agirrezabala and Dinarès-Turell, 2013; Agirrezabala et al., 2013, 2014; Wiese et al., 2015; Jakubowicz et al., 2021, 2022). At a larger scale, the question relevant to the impact of numerous magmatic intrusions on marine carbonate environment and on ecosystems above such structures remains open.

2 Geological setting

2.1. Structural context and magmatic occurrences

The Basque-Cantabrian Basin (BCB) is a 250 km long and 100 km wide well-preserved hyper-extended basin (**Fig. 1**) resulting from oblique rifting that occurred from the Late Jurassic to the Early Cretaceous at the Iberian-European plate boundary. The BCB was later mildly inverted by the subsequent Pyrenean orogeny which occurred from the Santonian to the Oligocene (Lagabrielle et al., 2010; Roca et al., 2011; Tugend et al., 2014; Pedrera et al., 2017, 2021; García-Senz et al., 2020).

During the late hyper-extended rifting phase in Early Cretaceous, the Central BCB was seated on an extremely Weise continental lithosphere (**Fig. 1B**) with some patches of exhumed mantle (Mendia and Ibarguchi, 1991; DeFelipe et al., 2017; Pedrera et al., 2017), related to a high-temperature metamorphic event (Clerc et al., 2015; Ducoux et al., 2021) and resulting in widespread metasomatism and hydrothermalism (Agirrezabala, 2009, 2015; Jakubowicz et al., 2021), as well as volcanism within the basin and on the seafloor.

This Early Cretaceous magmatism (especially during the Albian) is currently exposed at the surface and is expressed by both intrusive bodies and by extrusive volcanic complexes of lava flows or volcaniclastic deposits (Rossy, 1988; Fernández-Mendiola & García-Mondéjar, 1995, 2003; Castañares, et al., 1997; Agirrezabala et al, 2017; Agirrezabala, 2015; García-Mondéjar et al., 2018). The magmatism was also identified through seismic data, especially along the present-day coastal area between Bilbao and Donostia San Sebastian (Agirrezabala & Dinarès-Turell, 2013; Agirrezabala et al., 2013).

During the Aptian-Albian, the central BCB was controlled and delimited by a set of NW-SE mainly extensional structures, in particular by the Bilbao fault zone (García-Mondéjar et al., 2018) where the study area is located (**Fig. 1A**). This fault zone, with indisputable

synsedimentary tectonic activity as demonstrated by García-Mondéjar et al. (2018), delimited the northern structural margin of several Urgonian platforms (**Fig. 2**), bordering the southern part of the subsiding area named the Biscay Synclinorium (**Fig. 1B** & **Fig. 2**) mostly filled with offshore sediments (Fernández-Mendiola, 1987; García-Mondéjar, 1990, 1996).

Igneous bodies are common along the Bilbao fault zone where the shallow crustal level is connected with the deepest part of the crust and the exhumed mantle (García-Mondéjar et al., 2018). These igneous bodies occur in Early Valanginian to Late Albian sediments which exhibit diverse facies (see **appendix A**), from neritic carbonates facies to relatively deep shale deposits (García-Garmilla & Carracedo-Sánchez, 1989; Garrote Ruiz et al., 1990; García-Mondéjar et al., 2018). The magma evolved mostly into basalts and trachytes, with mineralogical and chemical compositions typical of an alkaline sequence (Rossy, 1988; Carracedo-Sánchez et al., 2012). These magmatic episodes were dated using either K-Ar and Ar-Ar methods on amphiboles or biotites from the igneous bodies (Montigny et al., 1986; Ubide et al., 2014; García-Mondéjar et al., 2018), or by biostratigraphy and lithostratigraphy of the surrounding sedimentary strata in the case of volcanic events on the seafloor (Robador & Garcia de Cortazar, 1986; Fernández-Mendiola & García-Mondéjar, 1995, 2003). On this dataset (see **appendix A**), García-Mondéjar et al. (2018) observed that, in and near the Bilbao fault zone, older (Early Valanginian to Early Albian) magmatic events are located to the southwest where they usually intruded Urgonian carbonates whereas younger ones (Late Albian) developed north-eastward, mostly in offshore sediments.

Active salt tectonic associated with this rifting and volcanic trend, also take place by remobilization of the underlying Triassic salts in the BCB (**Fig. 1B**). This halokinesis is well recorded by diapirs or salt injections along faults causing inflation and folding of the overlying lower Cretaceous sediments (e.g., García-Mondéjar et al., 1996; Quintà et al., 2012; Bodego et al., 2018; Motte et al., 2021; Roca et al., 2021). However, along the Bilbao fault zone, the Early

Cretaceous halokinesis is not well marked although there is some evidence, including in the immediate vicinity of the study area (Antiguedad et al., 1983; Fernández-Mendiola & García-Mondéjar, 1983; Fernández-Mendiola, 1987; Gomez-Perez et al., 1994).

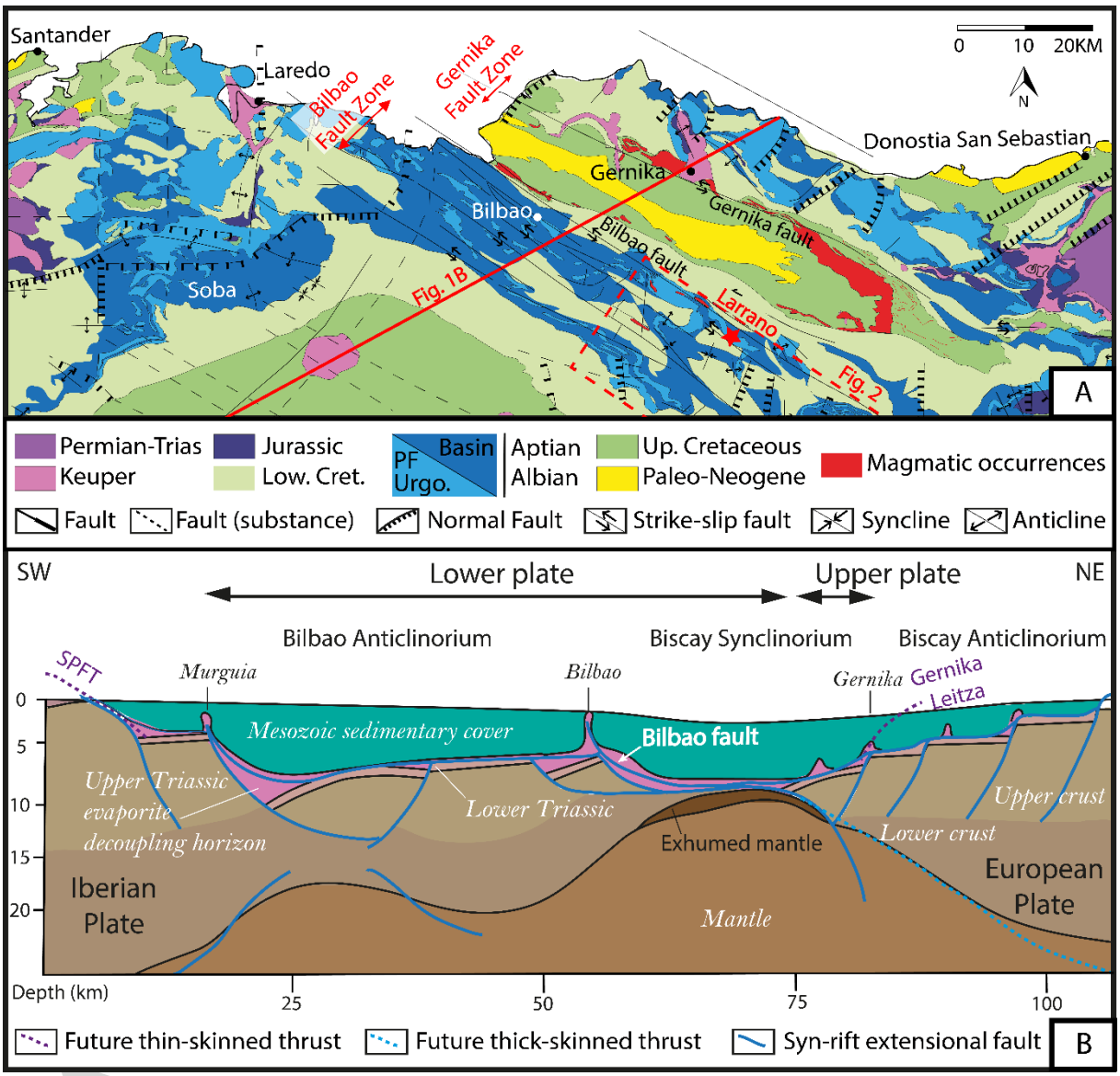

Figure 1: (A) Simplified geological map of the BCB with ages, main tectonic structures and magmatic occurrences. The abbreviation 'PF Urgo.' refers to '*Urgonian*' carbonate platforms. Compiled from Robador & García de Cortazar (1986); Fernández-Mendiola (1987); García-Mondéjar (1990); García-Mondéjar et al. (1996); Nader et al. (2012); Abalos (2016); García-Mondéjar et al. (2018). The study area of Larrano is indicated by a red star. (B) Reconstructed section across the BCB (cf. 1.A for location) during the late Cenomanian (Late rifting stage) highlighting the architecture of the continental lithosphere. SPFT for South Pyrenean Frontal Thrust. Modified from Lescoutre & Manatschal (2020). The study area lies along the Bilbao fault but is located southeast of this section.

2.2. The Duranguesado Carbonate Platform

The present study focuses on a magmatic event that occurred in the isolated carbonate platform of Duranguesado (*sensu* Fernández-Mendiola, 1987) and developed along the Bilbao fault zone, 40 km south-east of Bilbao (**Fig. 1A**). This isolated platform has a digited geometry (**Fig. 2**) and was bordered southward by shallow marine clastic deposits (siltstones and sandstones) of the Arlaban formation (*sensu* Fernández-Mendiola & García-Mondéjar, 1990), and northward by offshore shales and gravity deposits of the Bilbao formation deposited in the subsiding Biscay Synclinorium (see **Fig. 1A**, Fernández-Mendiola & García-Mondéjar, 1990; García-Mondéjar, 1990). The sedimentology and biostratigraphy of this platform were first studied by Rat (1959), and then further detailed by Pascal (1985), Fernández-Mendiola & García-Mondéjar (1983, 1990), Fernández-Mendiola, (1987). With facies from the "Urgonian Complex" (*sensu* Rat, 1959), this isolated carbonate platform was clearly separated by clastic deposits from other regional carbonate platforms (Fernández-Mendiola & García-Mondéjar, 1990) such as the nearby small isolated platforms of Zaraya and Udalaitz (**Fig. 2**).

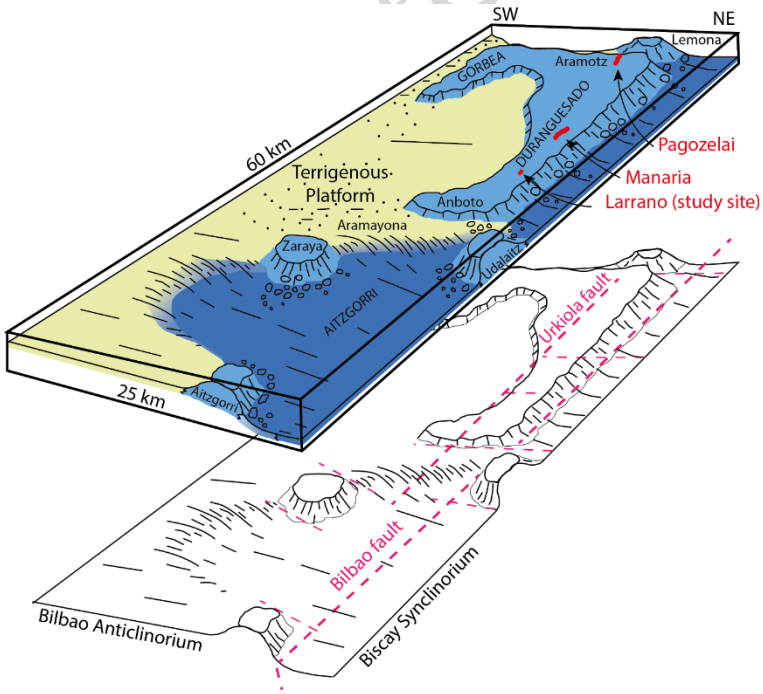

Figure 2: Architecture of the Urgonian carbonate platforms during the Early Albian, along the Bilbao fault zone in the Central part of the BCB (see Fig. 1A for location). Modified from Fernández-Mendiola & García-Mondéjar (1990) and Fernández-Mendiola & García-Mondéjar (2003). Pagozelai, Mañaria and Larrano are Early Albian magmatic events that occurred in the Duranguesado carbonate platform (Robador & Garcia de Cortazar, 1986; Fernández-Mendiola & García-Mondéjar, 1995; 2003).

From a stratigraphic standpoint, the Duranguesado carbonate platform lies on terrigenous facies (sandstone and siltstone) of the Tellamendi formation deposited during the Upper Aptian in an estuarine to tidal environment (Fernández-Mendiola & García-Mondéjar, 1989, 1991; Fernández-Mendiola et al., 1993). Immediately above it, the lower member of Aramotz formation (Upper Aptian to Earliest Albian) constitutes the basal part of the Urgonian series. The first limestone deposits form a progressive unconformity that pinches out southward (Fernández-Mendiola & García-Mondéjar, 1983; Fernández-Mendiola, 1987) and is now verticalized (**Fig. 3**). The northern border of the Duranguesado platform is thus clearly a structurally-controlled platform margin (Fernández-Mendiola, 1987; Fernández-Mendiola & García-Mondéjar,1983; 1990).

To the southeastern part of the Duranguesado platform (**Fig. 2**) the beginning of the Urgonian complex (Aramotz lower member) is characterized by the growth of a stacked reef-mounds, named the Anboto mound (**Fig. 3**), defined by Fernández-Mendiola, (1987). This author describes this structure as a set of decametric reef-mounds rich in coral-rudist strata. This composite mound is more than 400 meters thick and was bordered by well-expressed carbonate slopes, some of them steep enough to generate slumps and olistoliths (**Fig. 3**) as shown by Fernández-Mendiola & García-Mondéjar (1983) and Pascal (1985). During its first growth stages, the Anboto mound was probably an isolated mound in an offshore position relative to the main platform. At the Larrano site, about 1.8 km north-westward of the Anboto mound core, contemporaneous limestones of this mound (lower Aramotz member) were deposited on a lower slope setting (Fernández-Mendiola & García-Mondéjar, 2003). They are essentially massive to bedded mudstones or micro-wackestones with distal fauna such as crinoids and highly fragmented and micritized small bioclasts. At the Larrano pass, the Urgonian complex corresponds to the upper Aramotz member (Lower Albian), deposited after the growth of the Anboto mound (**Fig. 3**). This upper member is at least 700 meters thick, and is composed mainly

of mud-supported limestones, commonly showing fractured and non-fractured rudist shells. However, it may also contain other facies, such as boundstones with microbial *Bacinella* structures, floatstones with corals and rudists (requieniids, monopleurids, radiolitids), bioclastic packstones and rare bioclastic grainstones.

Finally, before a terminal angular unconformity and a sedimentary gap (Middle Albian is missing), the limestones of the Amarotz formation are overlain by the deepest sediments of the Bilbao formation (**Fig. 3**) due to the submersion of the platform (Fernández-Mendiola, 1987; Fernández-Mendiola & García-Mondéjar, 1990).

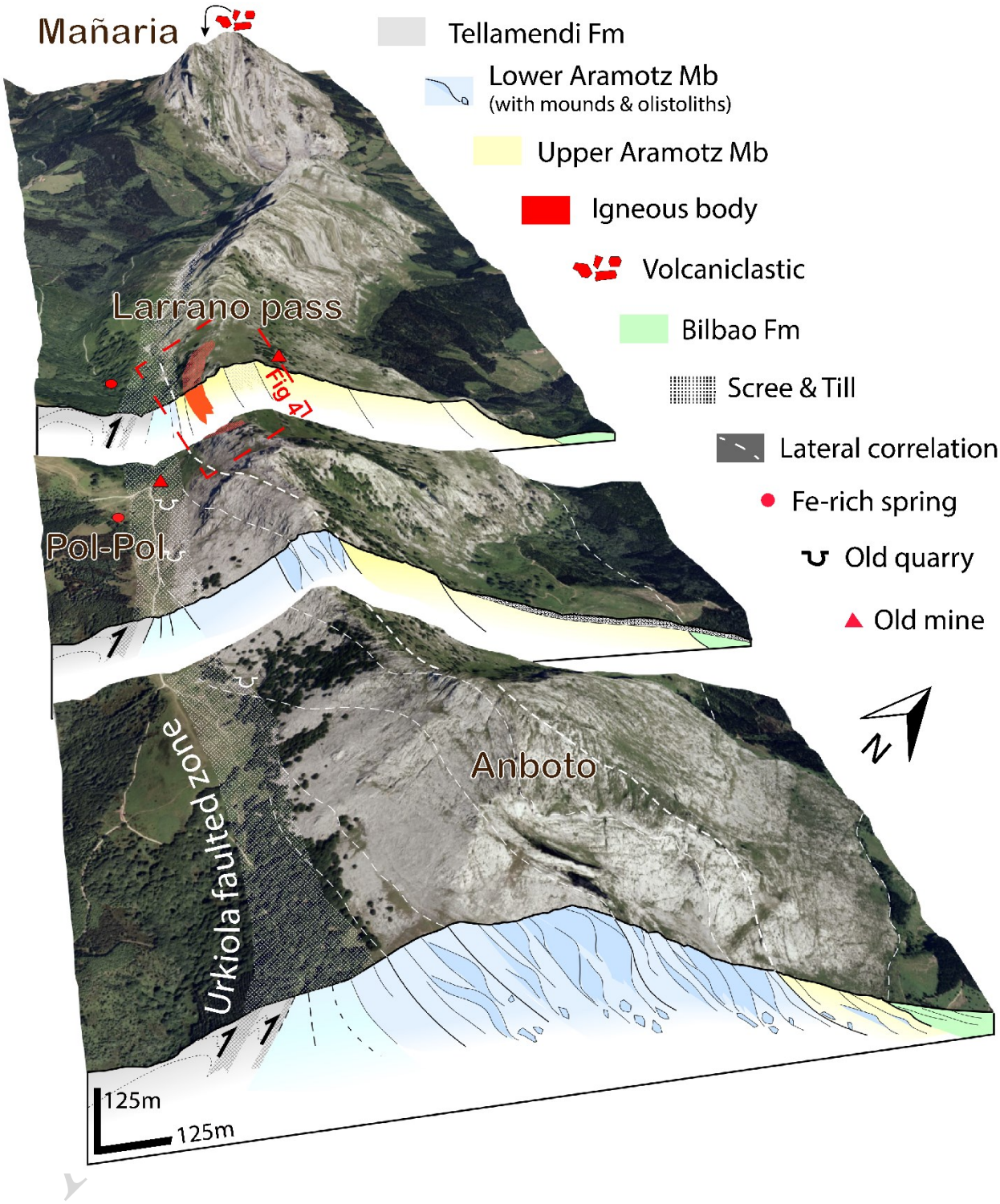

Figure 3: 3D outcrop view of the Larrano and Anboto areas showing sub-verticalized strata of the southeastern part of the Duranguesado carbonate platform. Screen & till refer to the Quaternary cover. Abbreviations 'Mb' and 'Fm' refers to 'member' and 'formation'. Satellite view and aerial images of 2011 from the ©2021 Eusko Jaurlaritza – Gobierno Vasco - Image Landsat / Copernicus database were used with Google Earth Pro software to the build this 3D block.

2.3. The Larrano igneous body and associated hydrothermal facies

Among the magmatic occurrences inventoried within the Duranguesado carbonate platform (**Fig. 2**), the Larrano igneous body is the largest and best known (Fernández-Mendiola & García-Mondéjar, 2003). These authors described a 'Y'-shaped basalt body that crosscuts the Urgonian strata, subsequently verticalized due to tilting. They also indicated that the basalts are fairly altered, especially in contact with surrounding limestones where a meter-thick altered clay-rich horizon is observed (see **appendix B**) but usually masked by a pedologic cover. Despite the high degree of alteration, probably due to both ancient hydrothermal and supergene alteration, primary basalt-forming minerals (e.g., plagioclase phenocrysts, amphiboles and pyroxenes) can be observed and are occasionally preserved within secondary mineralization (e.g., iron oxy-hydroxides, chlorite and calcite; see **appendix B**).

One of the main contributions of the previous study is the identification of specific sedimentary facies that preceded and followed the basaltic body emplacement. Fernández-Mendiola & García-Mondéjar (2003) described and mapped silicified beds, named "spiculites", in which sponge spicules are extremely abundant. Sponge spicules are cemented by a silicified matrix and are supported by each other, but rarely connected with each other. The authors suggested that these spiculites could be related to Si-rich seeps along fractures on the sea floor, modifying physicochemical parameters in the surrounding waters. Such hydrothermal-dependent sponge communities are observed in modern environments (Bertolino et al., 2017; Georgieva et al., 2020) and have been identified in ancient series (Bujtor & Nagy, 2021). At Larrano, other hydrothermally influenced facies are also suspected by Fernández-Mendiola & García-Mondéjar (2003). They consist of metric to decametric mud mounds or coral-rudist rich mounds where no chemosymbiotic biota have been identified, interstratified within sediments covering the basaltic body.

Based on their sedimentological, petrographical and geometrical dataset, Fernández-Mendiola & García-Mondéjar (2003) put forward a scenario for the emplacement and ensuing sealing of the igneous body. They describe initial hydrothermally influenced deposits along fault intersections, preceding the main magmatic activity. A subsequent eruptive event is then described, with two small, aerial volcanic cones which developed during exposure of the platform. They suggest that following the eruption, these volcanic cones would have been completely eroded and evacuated, probably under aerial conditions. This justifies the absence of any igneous rocks and minerals interstratified within the covering series. They adopt the hypothesis that the igneous body is a preserved 'Y'-shaped basaltic body and would therefore constitute the root of aerial cones that are now totally eroded. In a third stage, as the igneous root cooled, an increase in the subsidence rate would have promoted resumption of sedimentation that comprises both classic Urgonian limestone and hydrothermally influenced facies.

From a biostratigraphic standpoint, Fernández-Mendiola & García-Mondéjar (2003) indicated that the limestone surrounding the igneous body contains Early Albian benthic foraminifera fauna such as *Orbitolina (M) subconcava*, *Simplorbitolina manasi*, *Sabaudia minuta*, *Orbitolina (M) texana*, *Coskinolinella* sp. and *Cuneolina* ex gr. *Pavonia*, and especially *Orbitolina (M) subconcava* and *Coskinolinella sp.* into the hydrothermally-induced marine facies.

3 Material and methods

3.1. Field acquisition and sampling

Field investigations at Larrano-Anboto were carried out in two fifteen-day campaigns in August 2019 and in October 2020, for observations and sampling. 202 outcrop samples were collected as per regulations (permission n°AU-126-2020) and instructions of the Urkiola Natural Park. Sampling was conducted following a multi-scale strategy: (i) sampling at large intervals, encompassing the entire SE area of the Duranguesado carbonate platform, (ii) dense sampling focusing around the Larrano igneous body. In the field, facies mapping and a structural study were performed using GPS positioning together with detailed satellite / aerial images and orthophotography views from different years and seasons, to detect and delineate the lateral extension of the beds, unit boundaries and faults. The satellite images and orthophotography views were sourced from Sentinel-2 (Copernicus Sentinel data, 2021) and from the General Direction of Cadastre, Interministerial Flight @IGN PNOA (National Air Orthophotography Plan) 1973 to 2005.

3.2. Analytical methods

Facies characterizations were carried out on polished slabs and thin sections. Petrographic studies were done at the University of Burgundy (Gismo platform) with conventional methods. A set of 217 thin sections was described under plane-polarized light (PPL) and cross-polarized light (XPL) using a Nikon AZ100 macroscope coupled with a Tucsen TrueChrome 4K Pro camera and a Zeiss Axiophot microscope coupled with an Luminera Infinity 2-3C (3MP) camera. Additionally, UV-Epifluorescence microscopy was carried out on some samples using the same Nikon AZ100 macroscope. Alizarin red S and K-ferricyanide staining were used on thin sections especially for detection of Fe-rich calcite and dolomite crystals.

Cathodoluminescent microscopy (CL) was conducted on 102 polished thin sections using an ELM-3R luminoscope (12 to 20 kV gun potential, 0.7 to 1.3 µA beam current) coupled with a Leica Microscope MZ12 and a Tucsen Fl-20 camera.

Elemental mapping was conducted on samples of polished slabs and thin sections. Smaller elemental maps (7) and semi-quantitative spot analysis (93) were performed on key samples (gold-covered metallized thin sections) using a Jeol SEM JSM-IT100LA equipped with an EDS probe (University of Burgundy, Gismo platform). Additional elemental analyses were done using the SEM FEG QUANTA 650 FEI also equipped with EDS spectrometry for Elementary Analysis (TotalEnergies Laboratory, CSTJF - Pau, France) resulting in 11 elemental maps and 34 semi-quantitative spots analyses. Wider elemental maps were also performed using a micro X-Ray Fluorescence 2D scanner (Bruker M4 Tornado) composed of two SD detectors and a Cr X-ray tube anode with a polycapillary lens offering a 25 µm spot size (University of Burgundy, Gismo platform). This device was also use to measure elemental contents in cements (197 spots), sometimes in spots previously measured with EDS in order to inter-calibrate the two methods. A set of internal carbonate standards (whose elemental composition is known from ICP-MS measurements) was use to calibrate X-Ray Fluorescence values. The uncertainty is about 0,3 mol% for MgCO3 and 0,05 mol% for FeCO3.

Stable isotope analyses ($\delta^{18}O$ and $\delta^{13}C$, n=92) were conducted (University of Burgundy, Gismo platform) on selected thin sections hosting different phases of micritic matrix, bivalve shells with low magnesium calcite (LMC), calcite and dolomite cements. Two techniques were used to microsample the different carbonates, after cleaning with ethanol and purified water: (i) 55 samples were micro-drilled using a dental drill (with a drill bit of 500 µm in diameter) directly on the hand specimen (ii) 41 samples were micro-drilled on the unstained thin section under an x8 articulated lamp lens using a Proxxon MF70 microdrill device equipped with 300µm or 500µm diameter drill bits. Both techniques enabled us to obtain volumes of carbonate

powder of the order of 30 to 60 µg weighed with a Mettler Toledo XS3DU ultra-balance. A Kiel IV carbonate preparation device, paired with a Delta V Plus (ThermoFisher) mass spectrometer was used for isotopic analyses. Samples were dissolved at 70 °C by orthophosphoric acid, and isotopic values were calibrated relative to the NBS-19 standard. All stable isotope values are reported in per mil (‰) relative to Vienna Pee Dee Belemnite (V-PDB). The uncertainty associated to the measurement of $\delta^{18}O$ and $\delta^{13}C$ is ±0.1‰ and ±0.05‰ respectively.

In situ U-Pb radiometric dating was conducted at CEREGE (Aix-Marseille University) in the newly developed Laser Ablation Inductively Coupled Plasma Mass Spectrometry High Resolution (LA-ICP-MS-HR) laboratory facilities equipped with a 193nm Excimer laser (ESI) coupled to a sector field ICP-MS Element™ XR (Thermo Scientific™). U-Pb analyses were performed directly on polished thick (~100 µm) sections using a 150 µm laser spot size at low energy (fluence ~1J/cm^2 at 10Hz, see details on analytical methods in supplementary materials of Godeau et al., 2018). Samples were measured by a standard bracketing approach, using the NIST-614 glass standard for instrumental drift and lead isotope composition (Woodhead and Hergt, 2001) and the WC-1 natural calcite standard for inter-elemental fractionation (reference age = 254.4 ±6.4 Ma, Roberts et al. 2017). A second reference calcite, i.e., AUG-B6 (admitted age = 42.99 ±1 Ma; Brigaud et al., 2020) was also used to cross check element fractionation correction derived from WC-1 analyses. Five different calcite and dolomite cement phases, previously identified and mapped during PPL, XPL and CL examinations on 3 thick sections, were investigated. Spots (40 spot analyses) were positioned to analyse the different diagenetic phases. Detailed spot-by-spot assessment was carried out afterwards by examining ablation pits under CL microscopy. The U-Pb isochron ages were calculated using Isoplot software in order to plot the Tera-Wasserburg diagram (Discordia: model-1; Concordia: Tera-Wasserburg diagram).

4 Results

4.1. Geometries and strata layering at the Larrano site

As the present paper deals mainly with early deformation and diagenesis, we chose to not repeat the detailed description of sedimentary facies chronologically and spatially linked to the Larrano igneous body, previously studied by Fernández-Mendiola & García-Mondéjar (2003). However, to describe the different deformations and to precisely locate the diagenetic phases, a detailed layering model was required. This map integrates our field observations together with close examinations of various generations of aerial and satellite views (**Fig. 4**). It includes 9 successive stratigraphic units (**U1** to **U9**) separated from each other by rapid vertical facies variations such as is the case of pure limestone beds covered with marls or clayey limestones. Remarkable spiculite layers are also used to delimit some of these units, where locally they constitute the basal parts of units 2, 4, 6 and 7 (**Fig. 4**). Furthermore, the Larrano layering gradually disappears into the relative uniformity of the massive Urgonian facies, making it difficult or nearly impossible, to track it precisely over long distances beyond the Larrano pass.

4.2. Faults, folds and early deformations linked to the igneous body

Numerous faults and deformation structures around the igneous body were identified combining various generations of aerial and satellite views together with field observations. However, in the field, making close-ups of detailed observations of faults and associated deformations is not straightforward. They are three reasons for this: (i) the series is verticalized (**Fig. 3**), disturbing structural observations of the ground and making it necessary to use zenithal views; (ii) clay-rich soils linked to weathering of basalts, marls and silicified facies locally mask contacts between strata and fractures; (iii) numerous faults and deformations occurred before extensive lithification, so they affected partially-lithified rocks and are not associated with clear fracture planes, tectonic breccias or slicken-lines. These specific early deformations are

described below can be divided according to four categories: faults affecting more than 3 successive units, faults which only affect 1 to 3 units, folding and other deformations.

The main structure is a normal fault herein named the Santa Barbara fault (see a- in **Fig. 4A**). This fault exhibits a listric geometry and defines the base of the north-western limb of the igneous body, where the limestone-basalt contact is materialized by a yellow to brown clay-rich alteration profile, up to 3 meters thick. The offset related to this fault varies from one unit to another, attesting to its synsedimentary activity. The maximun offset (up to 30 meters) is observed at the tops of units 1 and 2. Offset values rapidly decrease upwards, becoming very low in the middle part of the unit 4, and ultimately inverted at the top of this unit. Then in units 8 and 9, the fault-related shift develops into fractures (**Fig. 4A**). Associated deformations, especially in the hanging wall, are flexible, forming notably a small roll over anticline in the unit 3 were spiculite beds are well expressed and close to each other (**Fig. 4A**). The deepest part of the Santa Barbara fault is largely masked by Quaternary deposits. Therefore, there is no direct evidence in favour of a connection with the underlying Urkiola fault. Otherwise the fault would pass just below an old lead mine and near the Pol-Pol Fe-rich spring (**Fig. 3**) where numerous fractures filled with calcite, dolomite and Fe-oxides crystals are observed in the terrigenous facies of Tellamendi formation. Eastward, another normal fault delimits the base of the south-eastern igneous limb (**Fig. 4A**). This fault exhibits relatively low throws affecting units 1 to 4 and is sealed by unit 5.

Many other minor faults were observed in this area, with limited throws and vertical extensions. In most cases they are small listric normal faults, with metric or sub-metric throws (**Fig. 4A**). Most of these faults developed in the upper part of units 2 and 3. A few of them also affected units 5 to 7. With few exceptions, most of these minor faults downfault toward the Santa Barbara fault, delimiting a subsiding zone called “small perched capping basin” (*by* Fernández-Mendiola and García-Mondéjar, 2003). This small depression is filled mainly with

clayey limestones, marls and well-expressed spiculite beds. Two other smaller troughs developed at the northwest and the southeast of the magmatic body. They are structured by small listric faults affecting units 2 and 3, filled by clayey limestones, marls and spiculite beds.

Finally, a last type of synsedimentary deformation is observed at the top of unit 4, between the two branches of the igneous body (details on **Figs. 4B** & **C**). These deformations disturb initially well-stratified marls and clayey limestones with small folds delimited by reverse faults forming duplex-like structures. Such synsedimentary deformations are only detected at the top of unit 4. Their geometry indicates beds sliding towards the hanging wall of the Santa Barbara fault, up to a buttress zone corresponding to the forced fold above the north-western branch of the igneous body (**Figs. 4B** & **C**). These deformations are sealed by unit 5 where onlaps are detected above the top of unit 4.

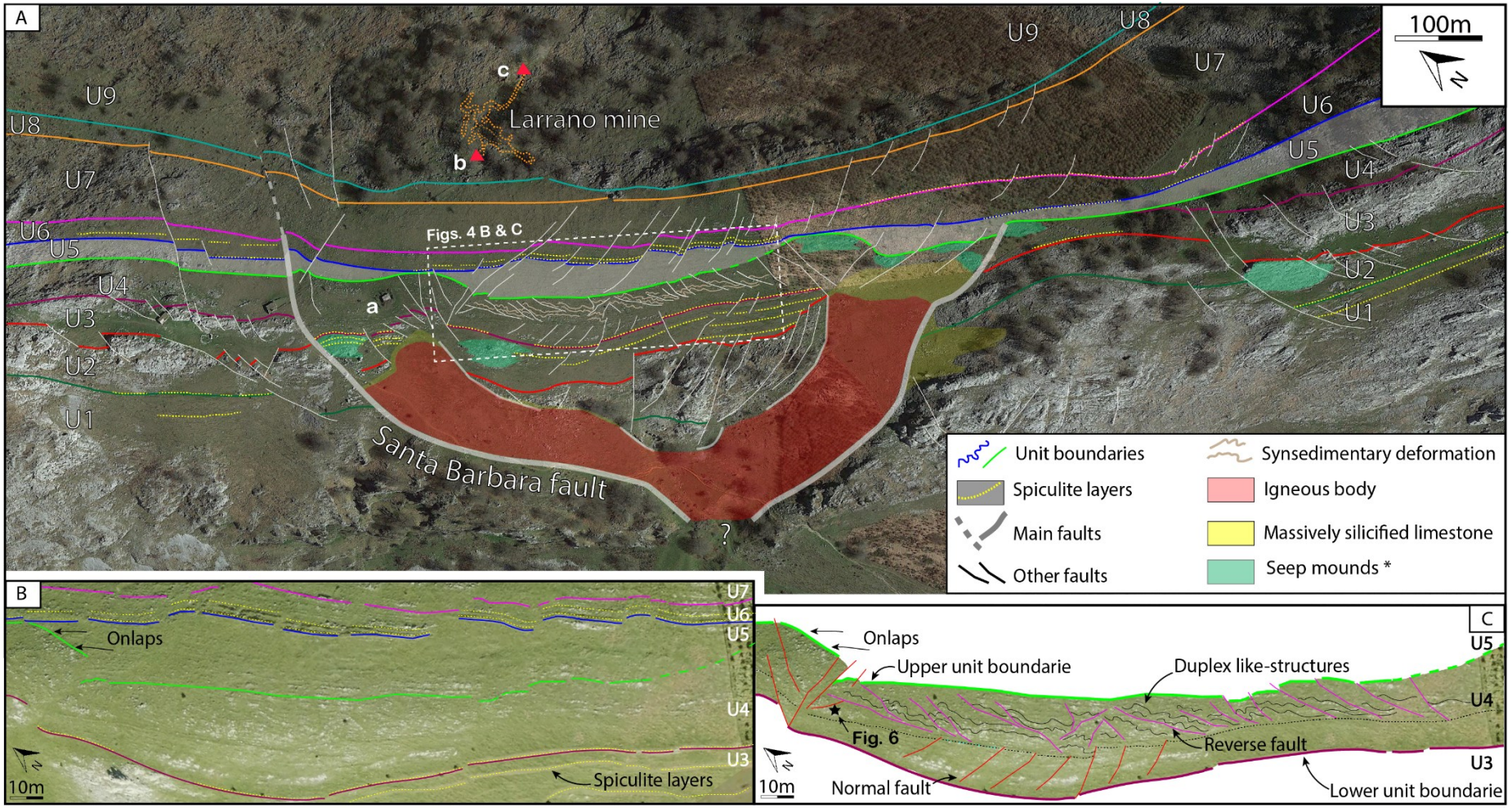
A
100m
U9
U8
U7
U6
U5
U4
U3
U2
U1
c
b
a
Larrano mine
Figs. 4 B & C
Santa Barbara fault
?
Unit boundaries
Spiculite layers
Main faults
Other faults
Synsedimentary deformation
Igneous body
Massively silicified limestone
Seep mounds *
B
Onlaps
Spiculite layers
10m
C
Onlaps
Upper unit boundarie
Duplex like-structures
Fig. 6
Reverse fault
Normal fault
Lower unit boundarie
10m

12

Figure 4: (A) Satellite view of the Larrano area (verticalized series) with the strata layering proposed in the present study. This layering includes 9 successive stratigraphic units (U1 to U9) delimited by color lines and affected by faults (thin to thick white lines). The extension of unit 5 is highlighted in grey. Extensions of spiculite layers are indicated by dashed yellow lines. a – the Santa Barbara hermitage; b, c, – upper and lower entrances, respectively, of the old Larrano Zn and Fe mine. Location of 'Seep mounds*' extracted from Fernández-Mendiola and García-Mondéjar (2003). Images from ©2021 Google, Images ©2021 Eusko Jaurlaritza – Gobierno Vasco, Maxar Technologies, ©IGN PNOA 1973 to 2005, together with 3D images from Google Earth Pro software (12/2021). (B) Undetailed and (C) detailed faults and deformations in unit 4. Red lines represent normal faults; pink lines correspond to reverse faults. Main deformations, with minor reverse faults (duplex-like structures) and crumpled limestone beds are observed in unit 4, between less disrupted unit 3 and overlying unit 5, highlighted by onlaps. See appendix C for more detailed image. Aerial images of 2004 taken from ©2021 ICV (Institute of Cartography of Valencia), ©2021 IGN PNOA (National Air Orthophotography Plan) 1973 to 2005, together with 3D images from Google Earth Pro software.

4.3. Diagenetic evolution and the Larrano eogenetic anomalies

Eogenesis

Isopachous calcite cements (ICC1a, b & ICC2) and aragonite dissolution

In the Larrano area, facies are predominantly mud-supported, moreover the macro porosity is limited. In this context, the Isopachous Calcite Cements (ICC) are very scarce. These cements are however detected in three distinct stratigraphic intervals: in unit 2 (ICC1a, **Fig. 5A**), at the top of unit 3 (ICC1b, **Fig. 5B**) and along fractures in unit 4 (ICC2, **Fig. 6**). The cement in these units form thin fringes of acicular to palissadic crystals of dirty calcite exhibiting cloudy brown to yellow luminescence under CL. In unit 2 and at the top of unit 3, these cements (up to 120 µm-thick) form thin fringes around allochems of the rare grainstone deposits (**Fig. 5B**) or precipitated on walls of moldic cavities due to very early dissolution of aragonite bioclasts (**Fig. 5A**). In unit 4, ICC2 cements are observed mostly in F2 fractures (**Fig. 6**), spatially and chronologically linked with duplex-like structures and highly deformed limestone beds (for location see **Figs. 4B** & **C**). There, ICC2 cement can be up to 350 µm-thick on the fracture walls but is thinner or absent in poorly connected pores bordering these fractures (**Figs. 6B** & **C**). Dissolution of aragonite bioclasts (corals, gastropods, parts of bivalves …) occurred several

times during eogenesis. Indeed, most of moldic cavities are filled or partially filled with eogenetic cements such as ICC or early blocky calcite spars.

First Blocky Calcite cements (BC1a & b)

In samples with primary or secondary macro-pores, the first Blocky Calcite cements (BC1 zone) occur as scalenohedral or syntaxial crystals of limpid calcite. In some cases, a BC1a subzone occurs in curved fractures (F1 in **Fig. 5E**) crosscutting the micritic matrix, corresponding probably to hydraulic fractures (*sensu* Jébrak, 1997). Depending on their superposition and their location in stratigraphic units U1 to U9, BC1 exhibits distinct subzones under CL and AF staining. The BC1a subzone, observed in units 1 to 4 (never above), is very dull luminescent under CL (dark brown to black) and is unstained by potassium ferricyanide (**Fig. 5A1**). Micro X-Ray Fluorescence measurements indicate an $FeCO_3$ content below 0.4 mol% and $MgCO_3$ content below 3.3 mol%. This BC1a subzone fills a major part of the macro porosity in close vicinity of the Santa Barbara fault. Elsewhere, BC1a is less voluminous (**Figs. 7E**, **7F** & **7I**) or absent. In unit 4, BC1a is clearly crosscut by F2 fractures (**Fig. 6B**). In a few samples, a thin band of Fe-rich calcite, stained blue by potassium ferricyanide, terminates the BC1a subzone.

No early blocky calcite cements are observed from unit 5 to unit 8. But, another subzone (BC1b) is detected around the lower entrance of the old Larrano mine (c- in **Fig. 4**), in unit 9. It shows strictly non-luminescent (black under CL) limpid calcite crystals (**Fig. 7G**), not-stained by potassium ferricyanide (Fe-poor calcite), growing directly on walls of primary pores or on walls of moldic pores after aragonite dissolution.

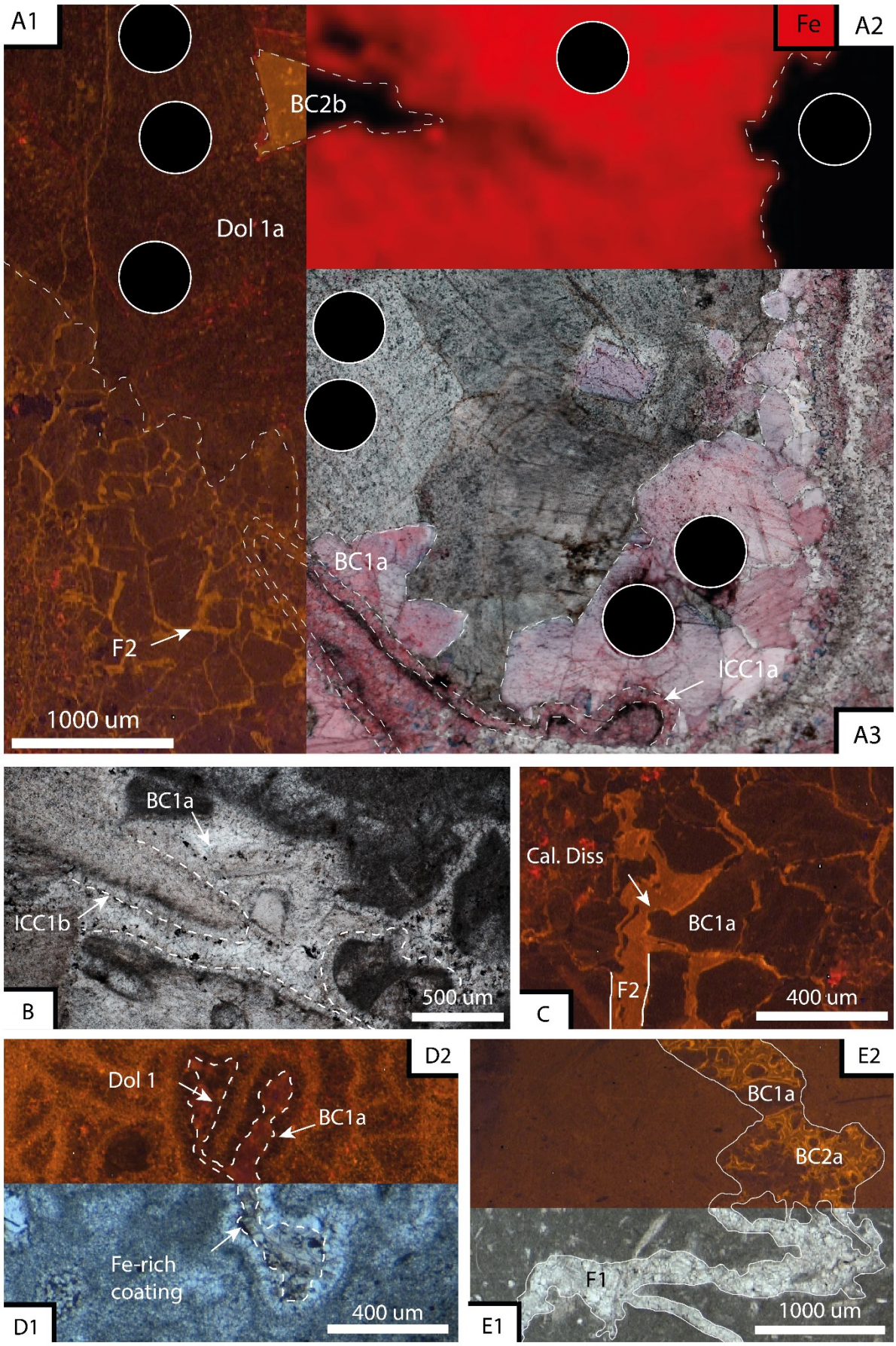
A1
Fe
A2
BC2b
Dol 1a
BC1a
F2
ICC1a
1000 um
A3
BC1a
ICC1b
500 um
B
Cal. Diss
BC1a
F2
400 um
C
D2
Dol 1
BC1a
Fe-rich
coating
400 um
D1
E2
BC1a
BC2a
F1
1000 um
E1

1

Figure 5: Main eogenetic phases in samples close to the Santa Barbara fault. (A) Composite image with CL (A1), Micro X-Ray Fluorescence elemental mapping with Fe-content in red (A2) and AF staining (A3) on micrographs. White circles with black fillings correspond to location of micro-drilled samples used for stable isotope analyses ($\delta^{18}O$ and $\delta^{13}C$). Cements precipitated in a moldic cavity due to very early dissolution of an aragonite bioclast. The isopachous ICC1a cement is the earliest cement detected here, overlapped by scalenohedral crystals the BC1a blocky calcite (Fe-poor), then by coarse saddle dolomite crystals of the Dol1 sub-zone (ferroan dolomite). Cataclastic micro-fractures (F2) crosscut BC1a before Dol1 precipitation and before calcite dissolution indicated by corrosion gulfs visible in (A1). Mesogenetic blocky calcite cement (BC2b) fills the remnant pore space. Sample from top of unit 2. (B) PPL micrograph with ICC1b isopachous cement forming thin franges around allochems in an unusual grainstone deposit. Pyrite crystals sealed ICC1b before BC1a. Sample from top of unit 3. (C) CL micrograph showing BC1a affected by cataclastic fractures (F2) and dissolution gulfs (Cal. Diss). Sample from same location as (A). (D) Composite image with PPL (D1) and CL (D2) micrographs of intra-skeletal cavities linked to *Bacinella* fabric. BC1a, Fe-rich coatings and finally ferrous dolomite (Dol1a) successively filled these cavities. Sample from unit 2. (E) Composite image of PPL (E1) and CL (E2) micrographs of a hydraulic (?) fracturing phase (F1) filled with successive BC1a and BC2a blocky calcite cements. Sample from unit 3.

The Larrano eogenetic anomaly

Five specific diagenetic phases are documented within a few meters around the igneous body and the Santa Barbara fault. Post-dated by BC1b subzone and then by earliest mesogenetic phases, these five diagenetic phases are very atypical of diagenesis occurring in marine platform carbonates in very shallow burial conditions. They are part of the "*Larrano eogenetic anomaly*" (**Fig. 8**) whose signification will be discussed later. All these atypical phases are recorded only up to unit 4, but never above.

The first atypical phase consists of intense cataclastic fracturing (F2 in **Figs. 5A1** & **C**) affecting bioclasts as well as ICC1a, ICC1b and BC1a cements (**Fig. 6B**). With a branched and anastomosed geometry, the microcracks are sometimes so numerous and close to each other that they can make it difficult to decrypt the initial microfacies. The second atypical eogenetic phase is a calcite-dissolution phase, particularly affecting the walls of some cataclastic microcracks, giving them a curved geometry, with corrosion gulfs (**Figs. 5A1, 5C**). Fe-rich coatings are also characteristic of this event, but they are only observed in samples very close to the igneous body. The Fe-rich coatings developed F2 microcracks here and on walls of intra-

skeletal cavities of *Bacinella*-rich limestones (*sensu* Pascal & Przybyla, 1989; Schlagintweit et al., 2010; Schlagintweit & Bover-Arnal, 2013; **Fig. 5D**). SEM observations, together with XRD measurements, reveal Fe-oxides and Fe-hydroxides, but these minerals may correspond to the replacement/alteration of Fe-rich precursors of unknown composition due to the likely influence of Quaternary weathering.

The following anomalous phase is a dolomitic (Dol1) cement precipitating over Fe-rich coatings (**Fig. 5D**) and unaffected by cataclastic F2 microcracks (**Fig. 5A1**). Under CL, Dol1 sometimes exhibits a first dull luminescent (black) subzone (Dol1a). This Dol1a cement may fill all the remnant macro-porosity with relatively coarse crystals (up to 4000 µm-thick) with curved faces and undulatory extinction under PPL. Dol1a is particularly well expressed around the igneous body and Santa Barbara fault where it can fill almost all the remnant porosity (**Fig. 5A1**). In pores around the igneous body, Dol1a cement exhibits a subhedral morphology (**Fig. 7A**). A more luminescent (dark orange) subzone (Dol1b) locally forms overgrowths on Dol1a (**Figs. 7A** & **C**), or it precipitated alone in the pores of unit 4(**Fig. 6**), exhibiting planar faces and sharp extinction (planar dolomite). AF staining (**Fig. 5A3**) and micro X-Ray Fluorescence indicate a Fe-rich dolomite (**Fig. 5A2** & **Fig. 7D**), especially in the dolomite crystal cores (Dol1a) where the $FeCO_3$ content is up to 10.1 mol%. Fe-content is lower in Dol1b subzone.

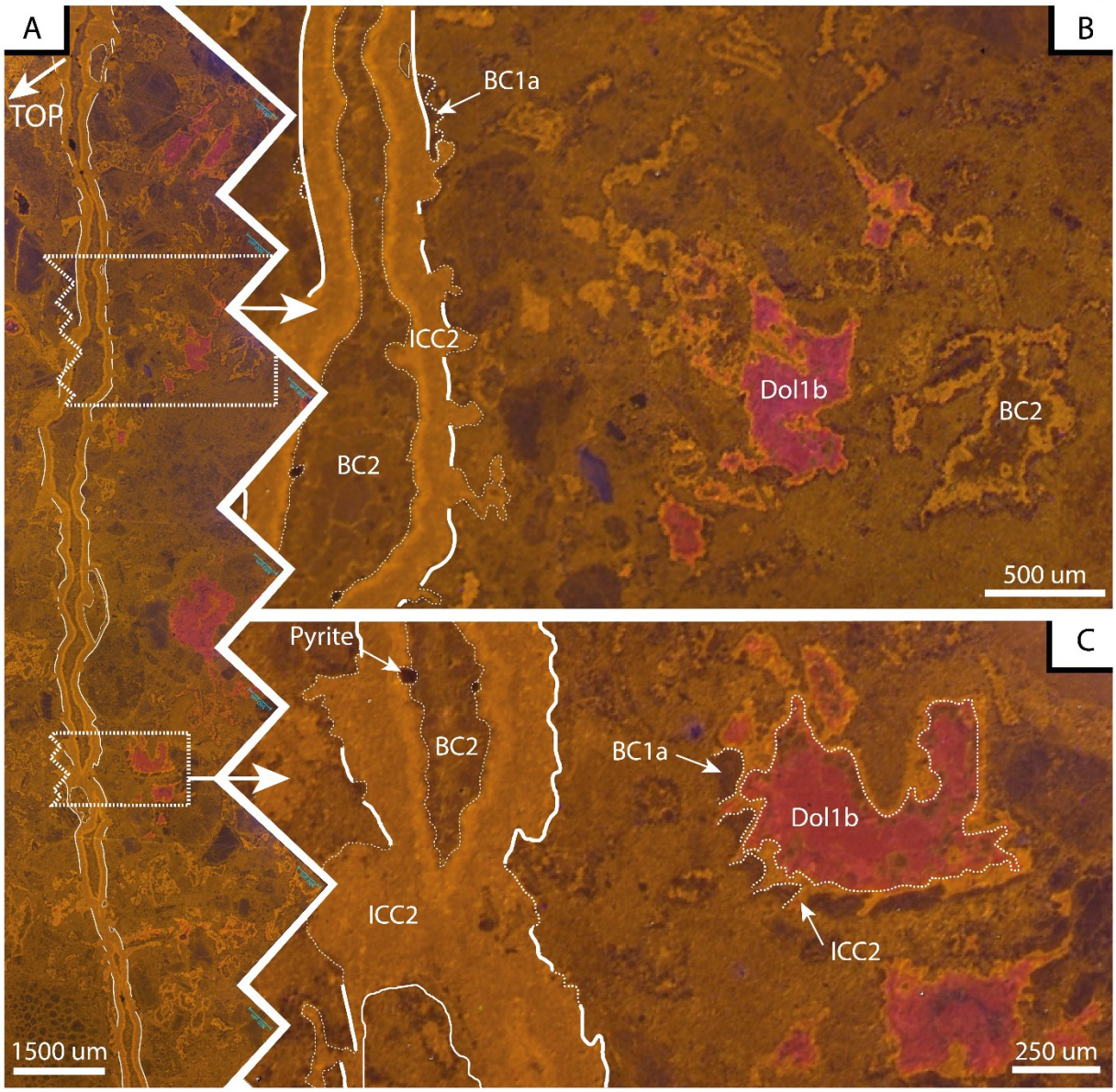

Figure 6: CL micrographs of diagenetic phases related to an F2 fracture at the top of unit 4, near the Santa Barbara fault. See figure 4C for location. (A) Global geometry of the F2 fracture (assemblage of 7 micrographs). (B) & (C) zooms reveal crosscutting of the BC1a cement by the F2 fracture (white line) then filled with successive ICC2, pyrite and BC2 cements. ICC2 cement reaches 350 µm-thick on fracture walls and is their major filling phase. ICC2 is a minor cement in the matrix porosity. Red-luminescent Dol1b cement precipitated in the remnant pores located away from the fracture, where ICC2 is thin.

Mesogenesis and Telogenesis

Except in areas around the igneous body and the Santa Barbara fault where BC1 and Dol1 cements may predominate, the most abundant cements are generally blocky calcite cements, named BC2 and BC3. They precipitated either in fractures, or in primary to moldic pores, sometimes after partial crushing and micro-fracturing due to lithostatic pressure. Such compaction features are not observed where earlier ICC, BC1 and Dol1 cements developed. In many samples, precipitation of these blocky calcite cements follows or is coeval with the precipitation of pyrite crystals (**Fig. 7I**), sometimes grouped into small framboidal structures.

BC2 developed mainly in limestones around the igneous body where it occludes the remaining porosity after ICC, BC1 and Dol1 cementing. Elsewhere, it is usually absent or thin (< 100 µm), poorly distinguishable from the overlying zone (BC3). In pores where BC2 is well developed, it is subdivided into two subzones (**Figs. 7E** & **7F**). BC2a is finely banded with alternating thin yellow to dark-brown bands under CL. It contains 1 to 3 Fe-rich bands (up to 0.9 mol% of $FeCO_3$) blue-stained by potassium ferricyanide, with occasional occurrences of small pyrite crystals (**Fig. 7I1**). Dog-tooth crystals of BC2a never exceeds 100 to 150 µm-long, especially observed in limestones around the igneous body. Elsewhere, BC2a is commonly absent, except in unit 9 where it forms very thin overgrowths on BC1b cements. BC2b is a Fe-poor calcite, unstained by potassium ferricyanide (**Fig. 7I1**), exhibiting an orange luminescence with some dull, low-contrasted thick bands (**Figs. 7E**, **7F** & **7H2**). Thicker than BC2a, its thickness can reach 700 µm.

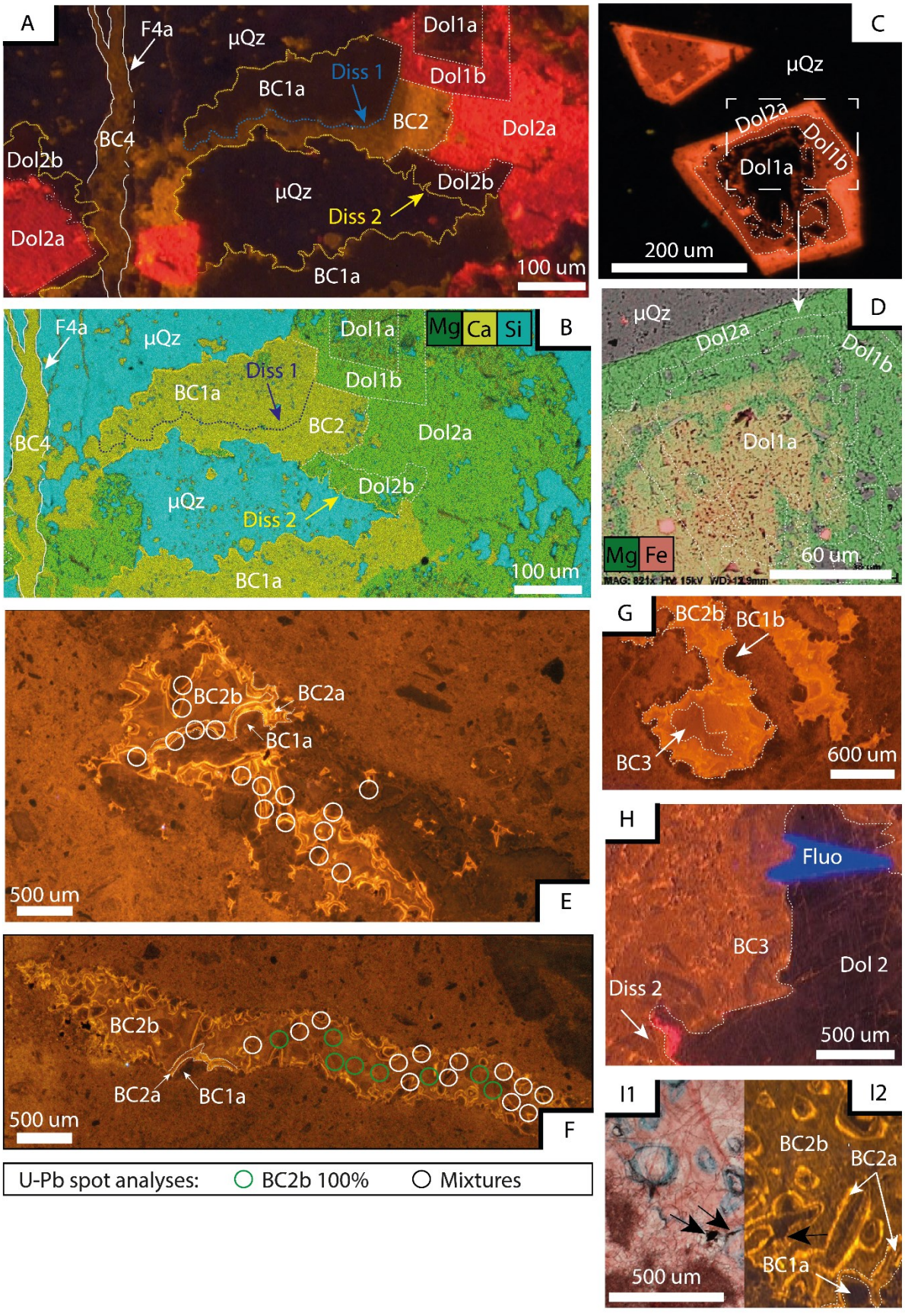
A
F4a
µQz
Dol1a
Diss 1
Dol1b
BC1a
BC2
Dol2a
BC4
Dol2b
µQz
Dol2b
Diss 2
Dol2a
BC1a
100 um
C
µQz
Dol2a
Dol1b
Dol1a
200 um
B
F4a
µQz
Dol1a
Mg Ca Si
Diss 1
Dol1b
BC1a
BC2
Dol2a
BC4
µQz
Dol2b
Diss 2
BC1a
100 um
D
µQz
Dol2a
Dol1b
Dol1a
Mg Fe
60 um
BC2b
BC2a
BC1a
500 um
E
G
BC2b
BC1b
BC3
600 um
H
Fluo
BC3
Dol 2
Diss 2
500 um
BC2b
BC2a
BC1a
500 um
F
I1
I2
BC2b
BC2a
BC1a
500 um
U-Pb spot analyses:
BC2b 100%
Mixtures

Figure 7: Some burial diagenetic phases.
(A & B) CL view and SEM elemental mapping of a unit 2 sample close to the Santa Barbara fault and the igneous body. Crosscutting relationships clearly reveal the relative chronology between BC1a, Dol 1a/1b, BC2, Dol 2a/2b, micro-quartz (µQz), fracture (F4a, bold white line) and BC4. They also reveal occurrences of dissolution phases between BC1a & BC2 (Diss 1, blue dashed line) and between Dol2b & micro-quartz (Diss 2, yellow dashed line).
(C & D) CL view and zoomed SEM elemental mapping of a spiculite bed in unit 3 sample near the Santa Barbara fault. Dolomite rhombs, with successive overgrowths including Dol1a/1b and Dol2a are perfectly encapsulated within micro-quartz (µQz) corresponding to silicification of the pre-existing micritic mud, thereby proving the anteriority of the dolomites to the silicification phase. SEM elemental mapping reveals the Fe-rich content of the dull luminescent Dol 1a subzone. (E & F) Moldic cavities filled with successive BC1a, BC2a and BC2b blocky calcite with U-Pb spots analyses (CL view). Sample from the top of unit 2 close to the Santa Barbara fault. (G) Successive BC1b, BC2b and BC3 filling a moldic cavity in unit 9 near the Larrano mine (CL view). (H) Sample of unit 5 close to the Santa Barbara fault showing successive precipitation of fluorite and Dol 2 cements sealing dissolution gulfs (Diss 2, white dashed line) affecting BC3 blocky calcite (CL view). (I) Composite image with AF staining (I1) and CL (I2) from a unit 4 sample close to the Santa Barbara fault showing Fe-rich bands and pyrite coating (black arrows) within BC2a subzone.

BC3 is the main blocky calcite cement in an area away from the igneous body and the Santa Barbara fault. It is not colored in blue by AF staining (**Fig. 7H**) but is slightly ferruginous (up to 0.3 mol% of $FeCO_3$). In some samples, BC3 is affected by a new generation of fractures (F3) and, more rarely, by dissolution gulfs followed by fluorite, the second dolomite cement with sub-zones (Dol 2 in **Fig. 7A**) or quartz (**Fig. 7H**). When Dol2 forms overgrowths directly on Dol1 rhombs, dissolutions gulfs are clearly observables under CL (**Fig. 7C**) or under SEM mapping (**Fig. 7D**).

Silicified limestones are relatively common in the Larrano area. They are divided into well-stratified spiculite beds and massively silicified limestones above the two limbs of the igneous body (**Fig. 4A**). The main silicified volumes are composed of micro-quartz crystals that replace a pre-existing micritic matrix (**Fig. 7C**). This replacement is readily observed where a silicifying front is preserved, for example at the boundaries of spiculite layers or of nodular cherts. Dolomite rhombs (Dol1 and Dol2 zones) are perfectly encapsulated within the micro-quartz replacement matrix (**Fig. 7C**), indicating that Dol2 predates the phase of silicification. The growth of this subhedral quartz, sometimes bipyramidal in shape, was locally hampered by

the presence of BC3 blocky calcite crystals, demonstrating, once again, the relatively late occurrence (post BC3) of the silicification. Fibrous quartz may also rarely occur in addition to micro-quartz and mega-quartz (observed in one sample of unit 2), precipitating over dissolution gulfs affecting the BC3 cements.

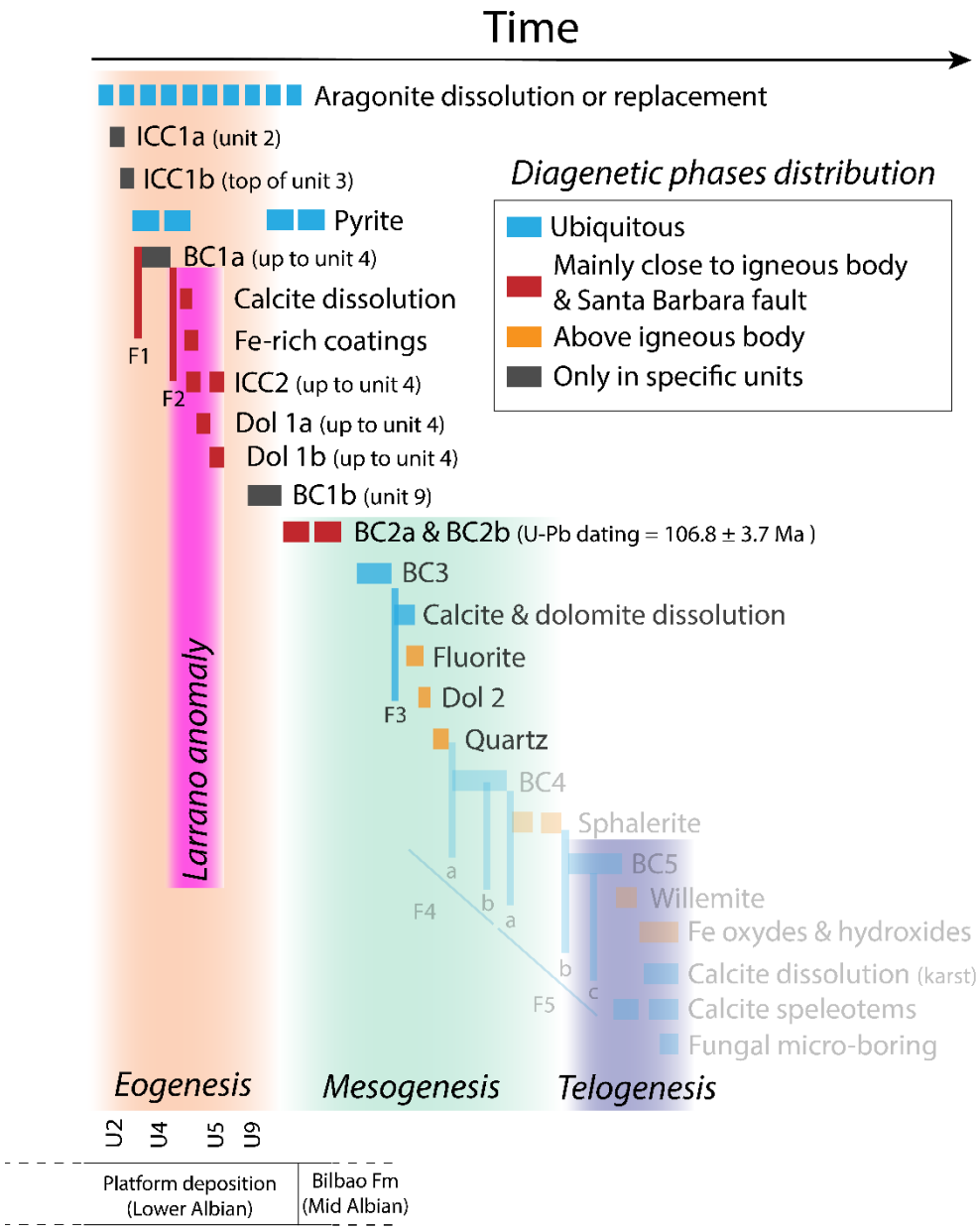

Figure 8: Diagenetic diagram for the Larrano area, compiling diagenetic data from 102 thin sections coming from stratigraphic units 1 to 9. Atypical phases in the eogenetic period are indicated as "Larrano anomaly". F1 to F5 indicate fracturing phases. ICC = Isopachous Calcite Cement; BC = Blocky Calcite cement; Dol = Dolomite cement (or replacement). See text for chronological correlation between diagenetic phases and sedimentary events. Late mesogenetic & telogenetic phases are detailed in appendix D.

4.4. Stable isotopes

Oxygen and carbon isotopic compositions were measured for 7 distinct diagenetic cements (BC1a, BC2b, BC3, BC4, BC5, Dol1 and Dol2) from the Larrano area, using micro-drilled samples (see part 3.2.). $\delta^{18}O$ and $\delta^{13}C$ from the micritic matrix and poorly recrystallized calcite of rudist shells were also measured (**Fig. 9**).

The earliest cements, BC1a (n=14) and Dol1 (n=12), have relatively similar $\delta^{18}O$ values (-7.5 to -6.1‰ for BC1a; -7.0 to -5.8‰ for Dol1), but distinct $\delta^{13}C$ signatures, with higher values for Dol1 (+3.6 to +4.3‰), than for BC1a (+2.2 to +3.5‰). The highest $\delta^{18}O$ and $\delta^{13}C$ values are measured on BC2b (n= 5), with -4.4 to -2.2‰ and +5.0 to +5.7‰ respectively. BC3 (n=9) has lower $\delta^{18}O$ values (-5.4 to -3.4‰) than BC2b and a $\delta^{13}C$ range (+3.2 to +4.4‰) that overlaps BC2b values, but with a lower average (+5.4 for BC2b vs +3.8 for BC3). The second dolomite cement Dol2 (n=2) presents very scattered $\delta^{18}O$ values and, to a lesser extent, $\delta^{13}C$ ranging from -10.9 to -4.0‰ and from +2.8 to +3.7‰ respectively. BC4 (n=3) has the lowest $\delta^{18}O$ and $\delta^{13}C$ values with -15.6 to -8.2‰ and +1.4 to +2.0‰ respectively. Finally, BC5 (n=3) values are quite similar to those measured in BC3, with a $\delta^{18}O$ ranging from -6.8 to -3.1‰ and a $\delta^{13}C$ from +3.1 to +4.7‰. In the micritic matrix (n=28) and rudist shells (n=16), $\delta^{18}O$ values range from -5.4 to -2.9‰ and -7.1 to -3.1‰ respectively and $\delta^{13}C$ values range from +2.7 to +4.7‰ and +1.4 to +4.7‰ respectively (see **appendix E** for more details).

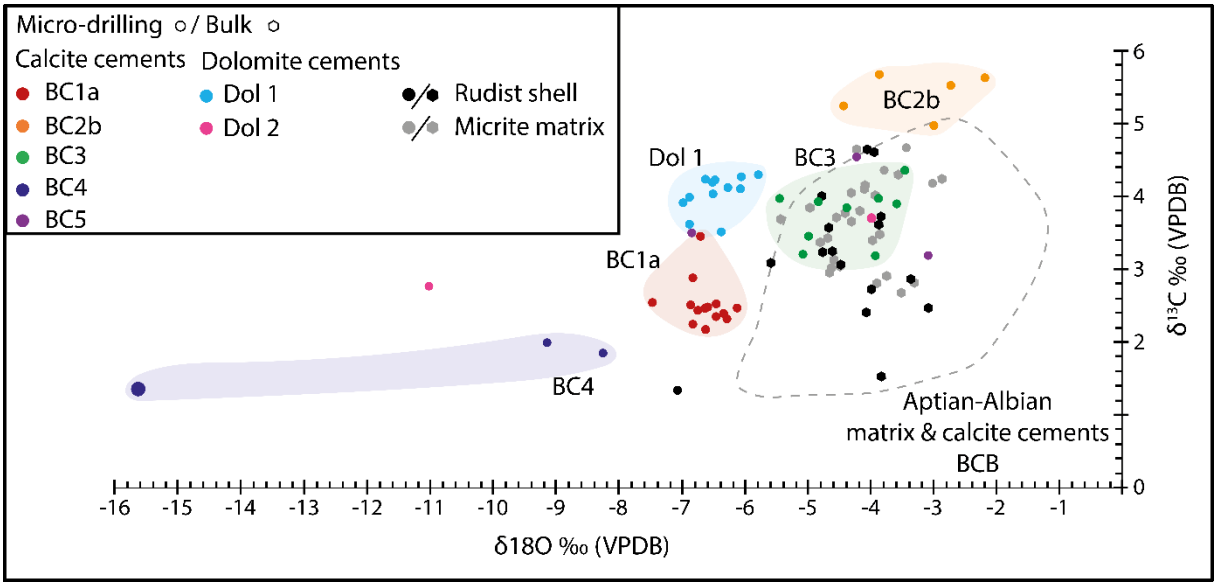

Figure 9: $\delta^{18}O$ versus $\delta^{13}C$ cross-plot from the Larrano area. It compiles data from thicker calcite cements (BC1a, BC2b, BC3, BC4 & BC5), dolomite cements (Dol1 and Dol2), micritic matrix and unrecrystallized rudist shells. The data is compared against previously published data from Aptian-Albian carbonate platforms (matrix and calcite cements) in the BCB (Bustillo et al., 1992; Fernández-Mendiola & García-Mondéjar, 1997; Neuweiler, 1993; Neuweiler et al., 1999; Aranburu et al., 2002; López-Cilla et al., 2012).

4.5. U-Pb Dating

In situ U-Pb radiometric dating were attempted on 3 thin sections, including 4 distinct calcites (BC1a, BC2, BC3, BC4) and 1 dolomite (Dol 1) cement. Of the three samples screened for U-Pb dating, only one sample provided sufficient U-Pb signal to be analysed with good accuracy. A total of 37 spot analyses were done on two distinct cemented vugs containing BC2a and BC2b calcite cements (**Fig. 7E** & **7F**). The whole data set shows good definition of a highly radiogenic pole close to the lower intercept of the Tera-Wasserburg diagram (**Fig. 10**), leading to the interpretation of a robust isochrone yielding a U-Pb age of 106.8 ±3.7 Ma.

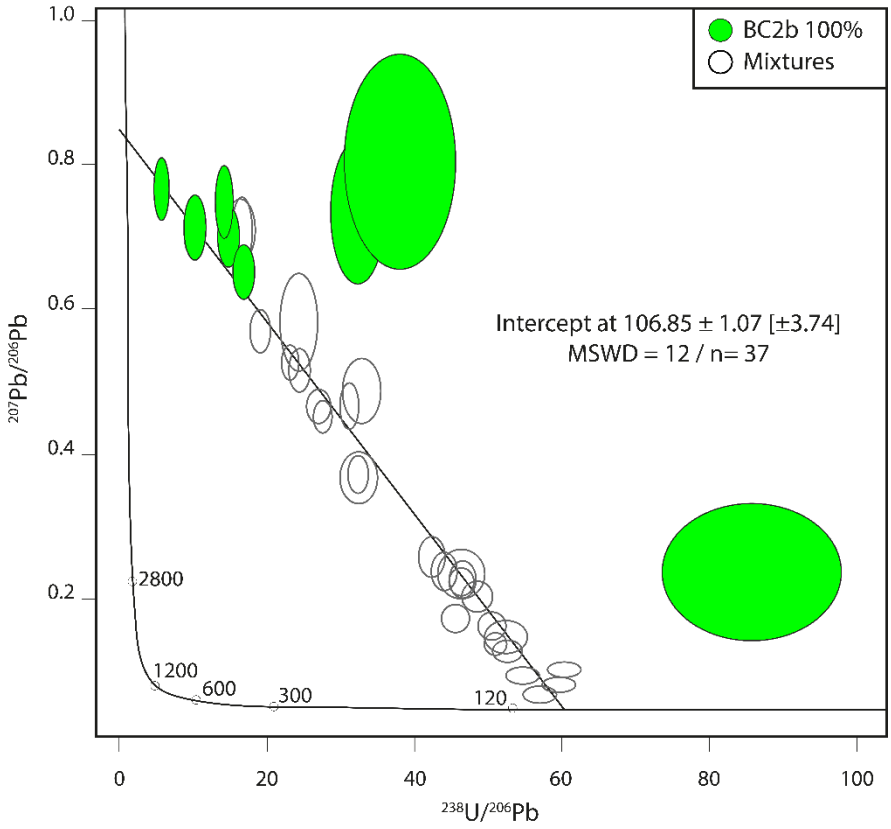

Figure 10: Results of *in situ* U-Pb radiometric analyses on BC2 cement presented on a Tera-Wasserburg diagram. The data yields a well-defined isochrone at 106.85 ±3.74 Ma. See (**Fig. 7E** & **7F**) for spots analyses location.

5 Discussion

The Larrano igneous body is an exceptional site for documenting the impact of a shallow sub-volcanic intrusion emplaced into a carbonate platform by using a method which couples sedimentological, structural, and diagenetic studies. This complete strategy allows us to specify the age and depth of the magmatic event and furthermore to characterize early diagenetic signatures as a consequence of magmatic emplacement (**Fig. 11**). One of the objectives of this chapter is to discuss what is really associated with this intrusion and what is linked to a classic diagenetic background (*e.g.,* meteoric / marine / burial). The hyper-extension of the BCB during the Aptian-Albian recorded many other magmatic episodes. The impact of numerous magmatic intrusions on the presence of a marine carbonate environment in a hyper-extended basin such as the BCB remains an open question. In fact, hyper-extended basins are defined by an

extremely thinned continental lithosphere, associated with some patches of exhumed mantle related to high-temperature metamorphic events (Clerc et al., 2015; DeFelipe et al., 2017; Pedrera et al., 2017; Ducoux et al., 2021). This geodynamic configuration would generate local to basin scale thermal anomalies (e.g. igneous intrusions vs. basin thermicity) possibly impacting fluid chemistry, ecosystems, and subsequent diagenesis.

5.1. Geometric and structural arguments for very shallow intrusion

According to Fernández-Mendiola & García-Mondéjar (2003) the igneous body of the Larrano site has been interpreted as the basaltic root of a small aerial volcano which extruded the carbonate platform before being eroded and then buried under new carbonate deposits. According to their scenario, these exposure, extrusive and erosive events would have taken place between the deposits of units 2 and 3 (**Fig. 4A**). During our field investigations and subsequent petrographic study of the numerous rocks samples, we found no traces of volcanic flows or volcanic breccias. Moreover, we did not find any volcanic rock fragments or igneous minerals reworked into the carbonate series. This type of evidence would be expected as the most direct proof of a synsedimentary effusive body, as recorded in many modern (Zinke et al., 2001, 2003; Nehlig et al., 2013) or ancient (Basile & Chauvet, 2009; García-Mondéjar et al., 2018) marine environments, including in carbonate series (Lokier et al., 2021). However, such evidence is lacking at the Larrano site. At the Mañaria quarry, 5 kilometres northward of the Larrano pass, volcanoclastic breccia are interstratified in carbonate layers of the Urgonian platform (Robador & Garcia de Cortazar, 1986; Fernández-Mendiola and García-Mondéjar, 1995), supposedly contemporaneous with the Larrano igneous event *sensu* Fernández-Mendiola and García-Mondéjar (2003). Of course, at Larrano, it can be argued that erosion could have eradicated all these traces before the onset of unit 3 sedimentation. It is also possible that volcanic products occurred only laterally, outside or aside of the outcrop zone, either in the southern part of the now eroded profile, or further north, in parts that do not outcrop. Another

argument in favour of volcanic events occurring just after unit 2 deposition was the absence of contact metamorphism on the limestones capping the igneous body. However, our diagenetic investigation does not support this interpretation, as similar early diagenesis is observed in limestones bordering the sides (units 1 and 2) and the top (unit 3) of the igneous body.

Considering the distribution of synsedimentary deformations in units 1 to 9, another scenario can be proposed (**Fig. 11**). The overall geometry of the depositional areas at Larrano, and the predominance of minor synsedimentary normal faults, clearly shows a predominantly extensional tectonics. This agrees with the regional geodynamic context of crustal thinning (**Fig. 1B**), demonstrated by a panel of sedimentary and tectonic evidence observed at many points of the BCB (García-Mondéjar et al., 1996, 2018; Aranburu et al., 2002; Bodego & Agirrezabala, 2007; Bodego et al., 2018; Ducoux et al., 2019). At the Larrano pass, additionally to common extensional features observed at many places in the BCB, other structures, sometimes compressive, are also detected especially in unit 4. First one are the two uplifted areas above the two branches of the igneous body, affecting units 2 to 4, sealed by later units with onlaps structures in unit 5 (**Figs. 4A** & **4B**). Others are the occurrence of highly deformed beds with minor reverse faults, duplex-like structures and small slump-like structures (underlying soft deformations) within unit 4, especially between the two uplifted areas (**Fig.4B**). These deformations occurred before complete lithification of the sediments (see parts 4.3 and 5.3) and these features are commonly used to clearly determine the stratigraphic position of a shallow igneous intrusion into a sedimentary column (Westerman et al., 2018). Several cases of buried igneous intrusions, both in clastic and carbonate series, had already been documented thanks to 2D and 3D seismic data (Breitkreuz & Rocchi, 2018; Bischoff et al., 2021). Some of them were outcropping (Morgan et al., 2008; Mathieu and Van Wyk de Vries, 2009) but few examples were found in carbonate platform environments. Based on this, and strengthened by analogical models (Abdelmalak et al., 2012; Galland et al., 2015), it can be put

forward that the deformations associated with unit 4, i.e., occurring during or just after its deposition, are linked to the rise of a viscous (?) basaltic magma along opening fractures, under shallow burial, in very poorly lithified and permeable limestones. Reverse faults and small folds in unit 4 (**Fig. 4B**) would thus result from limited bed slides along short, ephemeral slopes bordering the uplifted sediments (Mathieu and Van Wyk de Vries, 2009, Cruden et al. 2018; Hacker et al., 2018). According to this hypothesis, the Larrano intrusion would have ceased at very shallow depth just below the paleo-seafloor, corresponding now to the boundary between unit 4 and 5 (**Fig. 4A** & **11**). Above the two branches of the igneous body, the thickness between basalt tops (now very altered) and the top of unit 4 is about 45 meters as indicated by the thickness in **Fig. 4A**. This thickness is the lower estimate as we did not take into account the impact of compaction and erosion. Considering all these arguments, the Larrano igneous body is qualified here as a very shallow sub-volcanic intrusion, localized along the Urkiola fault (**Fig. 2**).

The 3D architecture of the Larrano igneous body remains unknown due to the absence of geophysical investigations, wells, caves or sinkholes below the Larrano Pass. The abandoned Larrano Fe - Zn mine, with its galleries and shafts (**Fig. 4A**, data provided by the Urkiola Natural Park), remains inaccessible, making it impossible to document the 3D geometry, because galleries of this mine are confined to unit 9 where ores occur in an “iron hat” over the igneous body. This iron hat is commonly caused by a hydrothermal body capping altered igneous rocks intruded into carbonate series (Hall et al., 1988). Nevertheless, a comparison of the Larrano igneous body geometries with other intrusions around the world, especially those occurring near synsedimentary normal faults, reveals important similarities with saucer-shape morphologies (Moller Hansen & Cartwright, 2006; Bischoff et al., 2021). Such intrusions need emplacement into non-to very weakly lithified sediments (Polteau et al., 2008), as was the case at Larrano. Among published examples of small saucer-shape intrusion emplaced at very

shallow depth, one case (Rui et al., 2013) shows striking similarity with the Larrano igneous body with an extensional context with numerous synsedimentary normal faults such as mega-scale faults and deformations in the pre-intrusive series, small half-grabens delimited by listric faults that developed at the periphery of intrusions.

5.2. Diagenetic signature of the shallow sub-volcanic intrusion

Diagenetic environment and fluid source

Considering the minimum estimated thickness of 45 meters between basalt tops and the top of unit 4, that allows us to qualify this intrusion as a very shallow sub-volcanic process, it can be argued that the diagenesis related to this event belongs to the very shallow burial domain. Moreover, this is corroborated by the lack of distinct compaction features (absence of crushing and collapse structures) before the precipitation of the BC2 cement (defined as post-intrusive in the following chapter).

In unit 4 as in other units of the Larrano pass, we did not observe any sign of vadose evidences such as anisotropic cements, paleo-karsts or paleo-soils features. This absence is consistent with the lack of main unconformities and the upper offshore depositional setting of these units. Moreover, the ICC2 cement is typical of neomorphosed High Magnesium Calcite (HMC) fibrous cements precipitating in marine phreatic conditions. Such cements commonly precipitated a few centimeters to a few decimeters below the sea floor, in cavities and fractures with a high Mg/Ca ratio in the flowing seawater, thereby providing Ca^{2+} and CO_3^{2-} ions for HMC precipitation (eg., Durlet & Loreau, 1996; Moore, 2001). Regarding the low amount of neomorphosed HMC cements, the depositional setting is consistent with the relatively distal depositional setting (external slope of the Urgonian platform) where HMC oversaturation is known to be low (e.g. Léonide et al., 2014; Godet et al., 2016).

Origin of pre-intrusive eogenetic phases

Before the intrusive event (**Fig. 11A**), the early diagenesis recorded in units 1 to 4 was characterized by sparse thin HMC isopachous cements ICC1 now neomorphosed to LMC followed by more widespread BC1a cements (**Fig. 8**).

BC1a is composed of limpid sparry calcite crystals with an initial low Mg content and mainly develops in floatstones with primary or secondary macro pores. In the literature, a similar cement is commonly reported as early sparite but its parent waters are variously interpreted as meteoric, marine or mixed. At the Larrano pass, in the upper offshore context of the units 1 to 8, we don't observe any clear sedimentary evidence of exposure during deposition. This is however not sufficient to exclude the intervention of meteoric or mixed waters during the early diagenesis, either because the exposure indices could have been eroded, or because such waters could come from emerged parts located further south and involved in submarine resurgences, possibly mixed with upward-rising fluids along fractures of the Santa Barbara fault. On the contrary, there is also no definitive proof that BC1a have a marine origin. Its $\delta^{13}C$ values (+2.2 to +3.5‰) fits well with a marine hypothesis, but it could also be compatible with a meteoric lens not associated with well-developed paleosoils as suggested for example in other Urgonian shelves (Godet et al., 2016). Taking into account this uncertainty about BC1a's parent waters, it is not possible to use its $\delta^{18}O$ signature to accurately calculate its temperature of precipitation. If the marine hypothesis is accepted, then BC1a precipitated from marine connate waters (34 to 52°C) as demonstrated by the calculation in **appendix F** based on the fractionation equation of Kim & O'Neil (1997) for calcite. If meteoric hypothesis is accepted, it would have precipitated without thermal anomaly (see also **appendix F**). Considering the absence of big bi-phase primary fluid inclusions in BC1a, perhaps only carbonate clumped isotopes (D47) measurements could solve this problem.

From a petrographic standpoint, the cement BC1a is widespread along the Santa Barbara fault representing a major synsedimentary fluid conduct and precipitated only near early fractures. This distribution could be consistent with the contribution of fluids coming along the Santa Barbara fault. Fernández-Mendiola & García-Mondéjar (2003) documented that hydrothermal-related facies (Si-rich fluids?) are deposited before magma emplacement, notably spiculite beds, the oldest of which are detected in unit 1 (**Fig. 4A**). According to these evidences, during pre-intrusive episodes, it could be considered that upward-rising fluids would have circulated through the most permeable parts of units 1 to 4.

Origin of the Larrano eogenetic anomaly

The Larrano eogenetic anomaly is clearly indicated by cataclastic fractures affecting bioclasts and BC1a cements that precipitated before the intrusive event. When a magma intrudes a sedimentary series, the first decimetres to meters of the host rock around the intrusion are impacted by local heating and over pressures, leading to the formation of a dense fracturing network in a damaged zone (Senger et al., 2015; Westerman et al., 2018; Sydnes et al., 2019). At Larrano, cataclastic fractures affect only local patches of micritic matrix (mainly mud-supported limestones). As observed in other hydrothermal systems, where distribution of early cement is commonly heterogeneous (Agirrezabala, 2009; Agirrezabala et al., 2013), this limited extent of cataclastic fracture suggests the matrix was probably not entirely cemented everywhere (Groshong, 1988; Cooke et al., 2018). Subsequent dissolution gulfs affected the walls of cataclastic fractures, just before, or at the same time as Fe-rich coatings. This indicates sudden, local circulation of Fe-rich waters relatively corrosive for calcium carbonate. Many studies focus on natural CO_2-rich fluids released from volcanic vents to understand the physical-chemical processes, in time and space, including parameters such as pH, CO_2 partial pressure (pCO_2), or carbonate saturation states (Barry et al., 2010), and thereby to estimate the environmental impact on such input. When CO_2-rich fluids are released, pCO_2 increases leading

to an increase in acidity and a decrease in carbonate saturation states (Hall-Spencer et al., 2008; Barry et al., 2010; Boatta et al., 2013). However, because these fluids rapidly interact with surrounding carbonate sediments, the acidity is quickly buffered, restricting calcite (or aragonite) dissolution to the proximal aureole (Lin et al., 2019). Mafic-derived fluids, particularly those rich in CO_2, have a strong iron concentration maintained in anoxic conditions (Boatta et al., 2013). Therefore, when such fluids are introduced into an oxidizing environment, iron oxy-hydroxides rapidly precipitate close to the fluid source (possibly through a microbial mediation/activation), as documented in many continental or marine volcanic settings, including in carbonate environments (Bougeault et al., 2019; Ferretti et al., 2019; González et al., 2020, Pascault et al., 2022).

During the settlement of the sub-volcanic intrusion, the associated thermal shocks and overpressures are quickly dissipated as demonstrated in numerous other studies of thermal effects caused by igneous intrusions (Tang et al., 2014). At Larrano, the thermicity of this anomaly can be estimated using the typology and isotopic composition of the dolomite cement (Dol1a, **Fig. 8**). As a reminder, the dolomite cement belongs to the eogenetic very shallow burial domain (see previous sub-chapter). The non-planar character of the dolomite crystal lattices is unusual in the "classical" eogenetic trends of marine carbonate series under very shallow burying because this lattice organization is usually interpreted to be indicative of temperatures over 55°C to 60°C (Sibley and Gregg, 1987), suggesting here a warm to hot water influence (Jacquemyn et al., 2014). Considering a $\delta^{18}O_{seawater}$ value of about -2 to 0‰ SMOW (Standard Mean Ocean Water) for the Early Albian seawater (Pearson et al. 2001; Pucéat et al., 2003; Prokoph et al., 2008), and using the Horita (2014) fractionation equation for dolomite, the temperature range obtained is about 51 to 70C° (**appendix F** for details). These estimated temperatures for a cement that precipitates in a very shallow depth before deposition of the unit 5 would imply a thermal anomaly, in agreement with the underlying magmatic intrusion.

In the overlying disrupted area, isopachous cements (ICC2, **Fig. 8**) are observed mostly in open fractures and in the few centimetres of macroporous limestones bordering these fractures (**Fig 6**). The fractures linked to the intrusive event acted as conduits for Mg-rich connate seawater rising up to the paleo-seafloor located at the top of the unit 4. These isopachous cements with petrographic characteristics of an initial HMC cement (**Fig 6**), precipitated very quickly in these fractures, in an ascending heated flow that could have been substantial. This precipitation may have started before the complete solidification of the underlying injected magma, when local thermal gradients were important, promoting a high flux of heated seawaters eventually mixed with upward-rising fluids. For kinetic reasons, this rapid precipitation would have favored HMC rather than dolomite. The second dolomite cement (Dol1b, **Fig. 8**) precipitating away from the igneous body (up to unit 4) is planar unlike dolomites located around the igneous body. In the overlying disrupted area, the isopachous cements (ICC2) are sealed by this Dol1b (**Fig 6**). This would suggest a lower temperature of Mg-rich connate seawater away from the igneous body, near the paleo-seafloor. This has occurred before the deposition of unit 5 since no such cements have been recorded above the top of the unit 4, in a probably cooling phase of the intrusion. This characteristic is consistent with the proposal of temperature gradient in the up-rising fluids, with significantly cooler flux near the paleo-seafloor rather than close to the igneous body (**Fig. 11B**).

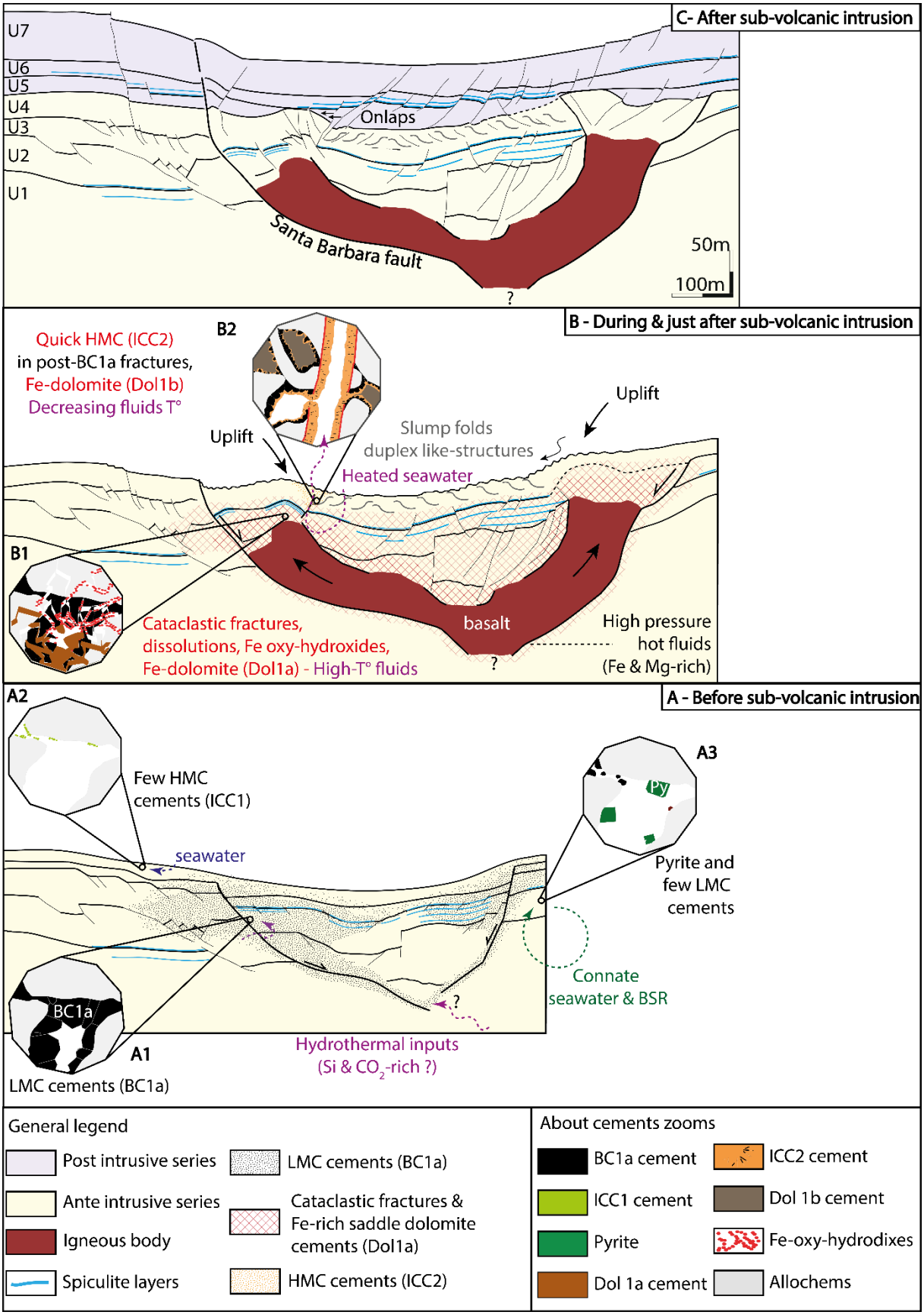
C- After sub-volcanic intrusion
U7
U6
U5
U4
U3
U2
U1
Onlaps
Santa Barbara fault
50m
100m
?
B - During & just after sub-volcanic intrusion
Quick HMC (ICC2)
in post-BC1a fractures,
Fe-dolomite (Dol1b)
Decreasing fluids T°
B2
Uplift
Uplift
Slump folds
duplex like-structures
Heated seawater
B1
Cataclastic fractures,
dissolutions, Fe oxy-hydroxides,
Fe-dolomite (Dol1a) - High-T° fluids
basalt
?
High pressure
hot fluids
(Fe & Mg-rich)
A - Before sub-volcanic intrusion
A2
Few HMC
cements (ICC1)
seawater
A3
Py
Pyrite and
few LMC
cements
Connate
seawater & BSR
?
BC1a
A1
LMC cements (BC1a)
Hydrothermal inputs
(Si & CO2-rich ?)
General legend
Post intrusive series
Ante intrusive series
Igneous body
Spiculite layers
LMC cements (BC1a)
Cataclastic fractures &
Fe-rich saddle dolomite
cements (Dol1a)
HMC cements (ICC2)
About cements zooms
BC1a cement
ICC1 cement
Pyrite
Dol 1a cement
ICC2 cement
Dol 1b cement
Fe-oxy-hydrodixes
Allochems

1

2

Figure 11: Simplified model for Larrano igneous body emplacement. (A) Before sub-volcanic intrusion emplacement (units 1 to 4), extensional stress, hydrothermal fluids may have promoted spiculite deposits at the surface (perhaps due to Si-rich fluid inputs) and LMC cements (BC1a) in sediments bordering the main fractures. Elsewhere, early diagenesis is limited to a few isopachous HMC cements and pyrite crystals, probably due do to BSR (bacterial sulfate reduction). (B) During and just after the sub-volcanic intrusion emplacement (unit 4). The intrusion caused local uplift, deformations (slump folds, duplex-like structures), erosion, as well as cataclastic fractures, dissolutions, Fe-rich coatings and Fe-rich saddle dolomites (Dol1a) around the igneous body. Contemporaneously, thick HMC cements (ICC2) precipitated along open fractures near the paleo-seafloor associated with dolomites (Dol1b) in vugs close to fractures. The Larrano eogenetic anomaly is highlighted in red. (C) After the sub-volcanic intrusion, units 5 to 7 progressively sealed the syn-intrusive structures (with onlaps in unit 5). Residual hydrothermal fluids may have promoted spiculite deposits at the surface (perhaps due to Si-rich fluid inputs).

Origin of post-intrusive shallow burial diagenetic phases

Among numerous mesogenetic to telogenetic phases recorded at Larrano, the earliest blocky calcite cement (BC2, **Fig. 8**) is interesting because it post-dated the Larrano eogenetic anomaly and provided a U-Pb age that accurately dates the paragenesis. Moreover, this age gives the possibility to replace this paragenesis in the burial curve and to discuss the intriguing very high $\delta^{13}C$ signature of BC2 cements.

From the *in situ* U-Pb radiometric dating obtained on BC2, the following observations can be made: (i) The robustness of the isochrone relies mainly on the highly radiogenic data points containing BC2a, which have the greatest weight on the calculated age. (ii) Data points including only BC2b do not bear much on the definition of the isochrone and the calculated age. (iii) The uncertainty on individual data points is very good overall in particular for the most radiogenic data points containing BC2a. (iv) The tree data points, scattered to the right of the isochrone come from pure BC2b and show a large uncertainty related to their very low amount of Pb (<10 ppb). These results lead to the conclusion that the isochrone depicted in **Fig. 10** gives a robust age and can be primarily attributed to the BC2a subzone. Considering uncertainties, the chronological range from 103 Ma to 111 Ma indicates that BC2a cement formed during the Albian, from the late Early Albian and the middle Late Albian. The

precipitation of this cement would therefore occur during, or just after, deposition of the last limestones of Duranguesado platform. A large uncertainty remains about the depth at which the cement BC2a precipitates, which may range from shallow marine environment to several hundred meters of burial depth (at least 700m, **Fig. 3**).

The very high $\delta^{13}C_{calcite}$ values (+5.0 to +5.7‰) measured in the mesogenetic BC2b subzone are relatively unconventional. They are not only the highest measured at Larrano, both in cements, bioclasts and bulk rock samples, but they are also values rarely recorded in calcite cements of carbonate platforms. Nevertheless, by listing all the $\delta^{13}C$ calcite published for the Urgonian bulk rock samples of the BCB and other peri-Pyrenean basins, it appears that positive excursions reaching up to +5 and even +6 ‰ exist in the Albian series. This is especially the case for the end of the Lower Albian, after the OAE 1a event, in the Aralar area (eastern BCB, Millán et al., 2014), maybe in relation with one of the major rifting tectonic pulse (II) of the BCB (García-Mondéjar et al., 2005). If considering that the high $\delta^{13}C_{calcite}$ values of BC2b are linked to deep circulation of late Early Albian marine water (during the positive carbon excursion), thus the oldest U-Pb age for BC2a (111Ma) need to be retained.

5.3. Comparison with other Albian igneous intrusions in the BCB

During Albian, the BCB evolved to a hyper-extended rift basin with numerous effusive and intrusive igneous bodies, especially along major fault corridors (García-Mondéjar et al., 2018; García-Senz et al., 2020; Jakubowicz et al., 2022).

A minor fraction of these intrusive/extrusive events occurred within Urgonian platform facies. Among them, Larrano is the only one where deformations and early diagenesis associated with the magma rise and cooling have been studied from samples located in the immediate vicinity of the igneous body. In other cases, the chronological and genetic relationships between possible magmatic intrusions within Urgonian platform facies and early

diagenetic phases has been suggested (García-Garmilla & Carracedo-Sánchez, 1989; Aranburu et al., 2002) but not sufficiently documented.

Geometric and diagenetic studies of magmatic Albian intrusions are located along the current coast of the Basque country (Agirrezabala, 2009, 2015; Agirrezabala and Dinarès-Turell, 2013; Agirrezabala et al., 2013, 2014; Wiese et al., 2015; Jakubowicz et al., 2021, 2022). In these studies, the link between early diagenetic phases and igneous bodies is well established. There, magmatic bodies generally intrude deep offshore deposits (shales and coarse-to-fine-grained turbidites of the Black Flysh Group), usually rich in organic matter. In their recent study, Jakubowicz et al. (2021) synopsized the geometries of these intrusions and their impacts on the geochemistry and diagenesis of the surrounding Albian sediments. They propose geometric models for magmatic sills occurring at different depths. Two sills, at Mutriku (Alkolea & Kardala) and Ispaster, intruded the sediments at original depths comprised between 1190 and 790 m (compacted). At Gorliz, the 'Larragan laccolith', emplaced in the upper part of Monte Grande Formation (Urgonian limestone) at a shallower depth (about 265 m, compacted), was followed by two subsidiary sills that are even more shallow (about 100m, compacted, Jakubowicz et al., 2021, 2022) and which intruded the Black Flysh Group. These emplacement depths are much greater than Larrano (45 m compacted) and resulted in different syn-intrusive manifestations at the paleo-seafloor. The most important sediment deformation occurs with the shallower igneous intrusion of Gorliz, where a syn-intrusive uplifted dome (forced folding) is detected (Agirrezabala, 2015). This dome is bordered by peripheral fractures, some of them filled with extruded breccia that include igneous rock fragments (Agirrezabala, 2015). At Larrano, syn-intrusive fractures reaching the paleo-seafloor also developed within and nearby uplifted sediments, even though, breccias with igneous fragments in their infilling were not detected. At the two other costal sites (Mutriku and Ispaster), the greater emplacement depths disfavored these types of deformations/extrusions. In fact, the synsedimentary signature

of intrusions within the Black Flysh Group consists of small patches of seep-carbonates developing at the paleo-seafloor or just below. These seep-carbonates are primarily identified by (i) the geological background; (ii) early diagenesis (brown anhedral calcite, fibrous calcite preceded and followed by several corrosion phases, Agirrezabala, 2009); (iii) occasional chemosymbiotic biota (Agirrezabala, 2009; Agirrezabala et al., 2013; Weise et al., 2015); and (iv) the Nd (Jakubowicz et al., 2021, 2022) and $\delta^{13}C$ signatures (Agirrezabala, 2009; Agirrezabala et al., 2013; Jakubowicz et al., 2021).

At Larrano, successive hydrothermally-influenced facies, notably spiculite beds (Fernández-Mendiola & García-Mondéjar, 2003) developed before and after the deposition of unit 4 that is, before and after the magmatic event (**Fig. 4A**). Moreover, metric to decametric carbonate mounds and biostromes (**Fig 4A**), some of them essentially micritic, are detected in units 2, 3 and 4. Although, no chemosymbiotic biota such as the carbonate seeps of the coastal sites, or specific eogenetic cements or mineralizations were identified in these carbonates. The influence of hydrothermal rises at the origin of their development (seep mounds) can nevertheless be considered, as proposed by Fernández-Mendiola & García-Mondéjar (2003).

At Larrano, the $\delta^{13}C_{carbonate}$ values are positive, both in micro-sampled early to late cements, in calcitic bioclasts and micritic matrices, thereby suggesting to the absence of thermogenic methane. This is an important difference between Larrano and the costal sills (Mutriku, Ispaster and Gorliz) where the lowest negative $\delta^{13}C_{carbonate}$ values (up to −41.6‰, at Ispaster) known from the studied Basque seeps are noticeable early isopachous cements (Agirrezabala et al, 2009), characteristic of carbonates formed due to oxidation of thermogenic methane (Agirrezabala et al., 2013; Jakubowicz et al., 2021). On the contrary, high positive $\delta^{13}C_{carbonate}$ values (up to +8.5‰, at Alkolea) are recorded in isopachous sparry calcite of the late diagenesis and are attributed to seeps expelling hydrocarbons of mixed origin, issuing biogenic, rather than thermogenic methane. Thus, these cements incorporate carbon derived

from residual, exceptionally ^{13}C-enriched CO_2 produced during microbial methanogenesis (Jakubowicz et al., 2021). This major ^{13}C-signature difference between Larrano and the costal sills (Mutriku, Ispaster and Gorliz) could be related to low concentrations of organic matter in the Urgonian facies of the Duranguesado platform and its basements (Fernández-Mendiola & García-Mondéjar, 1990; García-Senz et al., 2020). Without concentrations of organic matter, the sudden heating caused by the intrusion cannot have generated significant quantities of methane at Larrano. Therefore, the lithology of the igneous intrusion host rock, as well as its depth below the paleo-seafloor, play a key role in the very early diagenetic and geochemical signatures of these events, as already mentioned for many basins and settings (Agirrezabala, 2009; Aarnes et al., 2011; Svensen et al., 2018; Jakubowicz et al., 2021). Using a panel of geometrical, geochemical, sedimentological and diagenetical evidences, this paper demonstrates that Larrano is yet another example of this proposal.

Finally, it is important to discuss the common use of hydrothermally-influenced deposits as a chronological marker for an intrusive magmatic event (Mounji et al., 1988; Planke et al., 2005; 2018). At Larrano, successive hydrothermally-influenced facies, (Fernández-Mendiola & García-Mondéjar, 2003), developed before and after the magmatic event. This is another example that hydrothermal activity may occur before or after the igneous event itself (Belka, 1998; Jakubowicz et al., 2015).

Therefore, detection of hydrothermally-influenced facies is not always a robust method for relative dating of the magma emplacement. However, at Mutriku, Gorliz and Ispaster, the seep-carbonates are used to date the magmatic emplacements. This is a particular case where the very low $\delta^{13}C$ signature of some of these specific carbonates imply thermogenic methane, as a result of early heating of an underlying source rock, perfectly explainable by the thermal shock due to the magma rise.

6 Conclusion and Perspectives

During the Albian, the hyper-extended Basque-Cantabrian Basin was the seat of numerous magmatic phenomena forming either volcanic systems or magmatic intrusions at various depths. Before the present study, early diagenetic and geochemical signatures of such injections had been investigated, but essentially relevant to intrusions in deep clastic sediments. Such diagenetic impacts are less documented in carbonate platform sediments, not only in the Basque-Cantabrian Basin but also in other fossil to modern sedimentary basins. Using a range of complementary approaches and methods, we studied one such case of intra-platform magmatism, at the Larrano Pass, within the Duranguesado platform. For this emblematic case, we demonstrate the following points:

- The Larrano igneous body is composed of basalts (now fairly altered) which probably did not reach the surface at the location of the studied outcrop. This is consistent with the absence of any igneous clasts or lava flow interstratified within the surrounding and overlapping sediments. Intense deformations observed within an interval located about fifty meters above the igneous body testify to its very shallow emplacement within partially lithified mud-supported limestones.

- The very shallow occurrence of the intrusion is also attested by the "Larrano eogenetic anomaly". Along with cataclastic fractures, calcite dissolutions, Fe oxy-hydroxides, ferroan saddle dolomite and magnesian calcite, this anomaly forms a diagenetic overprint around the intrusion. The Larrano eogenetic anomaly is evidence of the thermal shock, overpressure and connate seawater circulation ($\delta^{18}O$ in saddle dolomite suggest temperatures of 51°C to 70C°) occurring at the time of and just after the magmatic intrusion.

- Upward-rising fluids circulation along fractures and normal faults also preceded and then followed the intrusive episode. A previous study (Fernández-Mendiola & García-Mondéjar,

2003) had already described occurrences of hydrothermally-influenced facies, notably spiculite beds. Here, we confirm the existence of the pre-intrusive upward-rising fluids circulation thanks to the characterization of an initial blocky calcite cement that precipitated only near early fractures, before the magmatic intrusion.

- The $\delta^{13}C$ positive values from various calcitic bioclasts, micrites and early cements (dolomite and calcite) at Larrano is consistent with the isotopic signature of Albian marine carbonate platform in the Basque-Cantabrian Basin. This trend diverges from other Basque-Cantabrian Basin cases where igneous intrusions occur within deeper Albian clastic deposits, where $\delta^{13}C$ signatures of seep-carbonates are mostly negative and consistent with thermogenic methane contribution. The scarcity of preserved organic matter in the Larrano igneous body host-rock (and below) did not favor such early thermogenic methane maturation.

The study of the Larrano outcrop has demonstrated that accurate dating of a very shallow magmatic intrusion in a carbonate platform may can be well constrained when all the sedimentological, structural, geochemical and eogenetic characteristics are compiled. This paper demonstrates that identifying hydrothermally-influenced deposits, near seeps above a magmatic body is not always a reliable approach for relative dating of an intrusion, because hydrothermal circulation may have preceded or followed the magmatic event.

Beyond this issue of dating accuracy, the influence of shallow magmatic intrusions on the production versus destruction of marine carbonates around intrusions (from local to regional scale) needs to be better understood. Certainly, magmatic-CO_2 is almost inevitably expelled into the sediments and then into the surrounding seawater. However, the role of magmatic-CO_2 contribution remains difficult to understand and quantify. At Larrano, the limited dissolution of calcite in cataclastic fractures bordering the magmatic body is consistent with the potential influence of natural CO_2-rich fluids released from volcanic vents. Further away in the surrounding carbonate sediments, the acidity is quickly buffered, restricting calcite (or

aragonite) dissolution to the proximal aureole. At this location, did magmatic-CO_2 boost the precipitation of carbonates, either by forming early cements, or by boosting the carbonate sedimentation rate in the neighboring environment? Finding the answer to this question will require further geochemical investigations, but as well as the study of modern cases where fluids linked to very shallow magmatic intrusions are still circulating in marine carbonate sediments.

Acknowledgements

This work was supported by TotalEnergies S.A, the company Akkodis and the Biogéosciences laboratory (University of Burgundy, CNRS). It is a contribution to the Akkodis-Biogeosciences convention (N°#2020-0443). The authors are grateful to Urkiola Natural Park for granting permission to collect samples in the field (N°AU-126-2020) as well as to Arantxa Bodego and Mikel López-Horgue (Universidad del País Vasco) for their help and useful scientific discussions during our field investigation. Gratitude is also express to the GISMO platform (Biogéosciences, University of Burgundy, UMR CNRS 6282) and its staff for their help on data acquisition (Pascal Taubaty, Théophile Cocquerez, Ivan Jovovic, Emilie Steimetz) as well as to the L1 laboratory staff from TotalEnergies S.A (Dimitri Richard, CVA-Group). Many thanks to Nicolas Godeau (CEREGE, Aix-Marseille University) and the R&D DATCARB program that granted permission to conduct U-Pb radiometric dating. The paper benefited expert editorial guidance from AngloFile. Thanks to Cathy Hollis and Benjamin Brigaud as reviewers for comments that have been helpful to clarify and improve this manuscript.

Author contributions - CRediT

Ophélie Pascault: Conceptualization, methodology, investigation, resources, writing – Original Draft, writing –Review & Editing, visualization, project administration. **Christophe Durlet:** Conceptualization, methodology, investigation, resources, writing – Original Draft, writing –Review & Editing, visualization, supervision, project administration, funding acquisition. **Pierre-Alexandre Teboul**: Software, investigation, writing –Review & Editing. **Maxime Ducoux:** writing –Review & Editing. **Jean-Pierre Girard:** Software, investigation, writing –Review & Editing. **Aurélien Virgone**: Conceptualization, investigation, resources, writing –Review & Editing, visualization, supervision, project administration, funding acquisition. **Thomas Saucède**: Conceptualization, investigation, resources, writing –Review & Editing, visualization, supervision, project administration, funding acquisition.

REFERENCES

Aarnes, I., Fristad, K., Planke, S., Svensen, H., 2011. The impact of host-rock composition on devolatilization of sedimentary rocks during contact metamorphism around mafic sheet intrusions. Geochemistry, Geophysics, Geosystems 12, 10. Q10019. https://doi.org/10.1029/2011GC003636

Abalos, B., 2016. Geologic map of the Basque-Cantabrian Basin and a new tectonic interpretation of the Basque Arc. International Journal of Earth Sciences 105, 2327–2354. https://doi.org/10.1007/s00531-016-1291-6

Abdelmalak, M.M., Mourgues, R., Galland, O., Bureau, D., 2012. Fracture mode analysis and related surface deformation during dyke intrusion: Results from 2D experimental modelling. Earth and Planetary Science Letters 359–360, 93–105. https://doi.org/10.1016/j.epsl.2012.10.008

Acocella, V., 2021. Volcano-tectonic processes. Ed, Advances in Volcanology. Springer International Publishing, Cham. 552p. https://doi.org/10.1007/978-3-030-65968-4

Agirrezabala, L.M., 2015. Syndepositional forced folding and related fluid plumbing above a magmatic laccolith: Insights from outcrop (Lower Cretaceous, Basque-Cantabrian Basin, western Pyrenees). Geological Society of America Bulletin 127, 982-1000. https://doi.org/10.1130/B31192.1

Agirrezabala, L.M., 2009. Mid-Cretaceous hydrothermal vents and authigenic carbonates in a transform margin, Basque-Cantabrian Basin (western Pyrenees): a multidisciplinary study. Sedimentology 56, 969–996. https://doi.org/10.1111/j.1365-3091.2008.01013.x

Agirrezabala, L.M., Dinarès-Turell, J., 2013. Albian syndepositional block rotation and its geological consequences, Basque–Cantabrian Basin (western Pyrenees). Geological Magazine 150, 986–1001. https://doi.org/10.1017/S0016756813000149

Agirrezabala, L.M., Kiel, S., Blumenberg, M., Schäfer, N., Reitner, J., 2013. Outcrop analogues of pockmarks and associated methane-seep carbonates: a case study from the Lower

Cretaceous (Albian) of the Basque-Cantabrian Basin, western Pyrenees. Palaeogeography, Palaeoclimatology, Palaeoecology 390, 94–115. https://doi.org/10.1016/j.palaeo.2012.11.020

Agirrezabala, L.M., Permanyer, A., Suárez-Ruiz, I., Dorronsoro, C., 2014. Contact metamorphism of organic-rich mudstones and carbon release around a magmatic sill in the Basque-Cantabrian Basin, western Pyrenees. Organic Geochemistry 69, 26–35. https://doi.org/10.1016/j.orggeochem.2014.01.014

Agirrezabala, L.M., Sarrionandia, F., Carracedo-Sánchez, M., 2017. Diatreme-forming volcanism in a deep-water faulted basin margin: Lower Cretaceous outcrops from the Basque-Cantabrian Basin, western Pyrenees. Journal of Volcanology and Geothermal Research 337, 124–139. https://doi.org/10.1016/j.jvolgeores.2017.03.019

Antiguedad, I., Cruz-Sanjulian, J., Fernandez-Mendiola, P.A., Garcia-Mondejar, J., 1983. Argumentos sedimentológícos e hidrogeoquímicos sobre la existencia de un diapirísmo de materiales triásicos en el área de Dima, Vizcaya. Boletín Geológico y Minero 94, 489–495.

Aranburu, A., Fernandez-Mendiola, P.A., Lopez-Horgue, M.A., Garcia-Mondejar, J., 2002. Syntectonic hydrothermal calcite in a faulted carbonate platform margin (Albian of Jorrios, northern Spain). Sedimentology 49, 875–890. https://doi.org/10.1046/j.1365-3091.2002.00475.x

Baarli, B.G., Cachão, M., da Silva, C.M., Johnson, M.E., Mayoral, E.J., Santos, A., 2014. A Middle Miocene carbonate embankment on an active volcanic slope: Ilhéu de Baixo, Madeira Archipelago, Eastern Atlantic : calcarenites on unstable slope of volcano. Geological Journal 49, 90–106. https://doi.org/10.1002/gj.2513

Barry, J.P., Hall-Spencer, J.M., Tyrell, T., 2010. In situ perturbation experiments: natural venting sites, spatial/temporal gradients in ocean pH, manipulative in situ pCO2 perturbations, in: Guide to best practices for ocean acidification research and data reporting. School of Biological and Marine Sciences 8. 123-136. http://hdl.handle.net/10026.1/1315

Basile, C., Chauvet, F., 2009. Hydromagmatic eruption during the buildup of a Triassic carbonate platform (Oman Exotics): Eruptive style and associated deformations. Journal of Volcanology and Geothermal Research 183, 84–96. https://doi.org/10.1016/j.jvolgeores.2009.03.009

Belka, 1998. Early Devonian Kess-Kess Carbonate Mud Mounds of the Eastern Anti-Atlas (Morocco), and Their Relation to Submarine Hydrothermal Venting. Journal of Sedimentology Research 68, 368-377. https://doi.org/10.1306/D42687B1-2B26-11D7-8648000102C1865D

Bertolino, M., Oprandi, A., Santini, C., Castellano, M., Pansini, M., Boyer, M., Bavestrello, G., 2017. Hydrothermal waters enriched in silica promote the development of a sponge community in North Sulawesi (Indonesia). The European Zoological Journal 84, 128–135. https://doi.org/10.1080/11250003.2016.1278475

Bischoff, A., Planke, S., Holford, S., Nicol, A., 2021. Seismic Geomorphology, Architecture and Stratigraphy of Volcanoes Buried in Sedimentary Basins, in: Németh, K. (Ed.), Updates in Volcanology - Transdisciplinary Nature of Volcano Science. 34-35. https://doi.org/10.5772/intechopen.95282

Boatta, F., D'Alessandro, W., Gagliano, A.L., Liotta, M., Milazzo, M., Rodolfo-Metalpa, R., Hall-Spencer, J.M., Parello, F., 2013. Geochemical survey of Levante Bay, Vulcano Island (Italy), a natural laboratory for the study of ocean acidification. Marine Pollution Bulletin 73, 485–494. https://doi.org/10.1016/j.marpolbul.2013.01.029

Bodego, A., Agirrezabala, L., 2007. Albian sediment-filled fissures on an Urgonian carbonate platform as kinematic indicators of extension, Westernmost Pyrenees. Geogaceta 41 of

2006, 27-30. ISSN 0213-683X.
Bodego, A., Iriarte, E., López-Horgue, M.A., Álvarez, I., 2018. Rift-margin extensional forced folds and salt tectonics in the eastern Basque-Cantabrian rift basin (western Pyrenees). Marine and Petroleum Geology 91, 667–682. https://doi.org/10.1016/j.marpetgeo.2018.02.007
Bougeault, C., Vennin, E., Durlet, C., Muller, E., Mercuzot, M., Chavez, M., Gérard, E., Ader, M., Virgone, A., Gaucher, E.C., 2019. Biotic–Abiotic Influences on Modern Ca–Si-Rich Hydrothermal Spring Mounds of the Pastos Grandes Volcanic Caldera (Bolivia). Minerals 9, 380. https://doi.org/10.3390/min9060380
Breitkreuz, C., Rocchi, S. (Eds.), 2018. Physical Geology of Shallow Magmatic Systems: Dykes, Sills and Laccoliths, Springer International Publishing. Ed, Advances in Volcanology. Springer International Publishing, Cham. 425p. https://doi.org/10.1007/978-3-319-14084-1
Brigaud, B., Andrieu, S., Blaise, T., Haurine, F., Barbarand, J., 2020. Calcite uranium–lead geochronology applied to hardground lithification and sequence boundary dating. Sedimentology 68, 168–195. https://doi.org/10.1111/sed.12795
Bujtor, L., Nagy, J., 2021. Fauna, palaeoecology and ecotypes of the Early Cretaceous sediment hosted hydrothermal vent environment of Zengővárkony (Mecsek Mountains, Hungary). Palaeogeography, Palaeoclimatology, Palaeoecology 564, 110-179. https://doi.org/10.1016/j.palaeo.2020.110179
Bustillo, M., Fort, R., Ordonez, S., 1992. Genetic implications of trace-element distributions in carbonate and non-carbonate phases of limestones and dolostones from western Cantabria, Spain. Chemical Geology 97, 273–283. https://doi.org/0009-2541/92/$05.00
Carracedo-Sánchez, M., Sarrionandia, F., Juteau, T., Gil Ibarguchi, J.I., 2012. Structure and organization of submarine basaltic flows: sheet flow transformation into pillow lavas in shallow submarine environments. International Journal of Earth Sciences 101, 2201–2214. https://doi.org/10.1007/s00531-012-0783-2
Cartwright, J., Santamarina, C., 2015. Seismic characteristics of fluid escape pipes in sedimentary basins: Implications for pipe genesis. Marine and Petroleum Geology 65, 126–140. https://doi.org/10.1016/j.marpetgeo.2015.03.023
Castañares, L.M., Orozco, S.R., Bravo, J.C.V., 1997. Distribución estratigráfica de los episodios volcánicos submarinos del Albiense-Santoniense en la Cuenca Vasca (sector Gernika-Plentzia, Bizkaia). Geogaceta 22, 43–46. ISSN : 0213683X
Clerc, C., Lahfid, A., Monié, P., Lagabrielle, Y., Chopin, C., Poujol, M., Boulvais, P., Ringenbach, J.-C., Masini, E., de St Blanquat, M., 2015. High-temperature metamorphism during extreme thinning of the continental crust: a reappraisal of the North Pyrenean passive paleomargin. Solid Earth 6, 643–668. https://doi.org/10.5194/se-6-643-2015
Cooke, A. P., Fisher, Q. J., Michie, E. A., Yielding, G. 2018. Investigating the controls on fault rock distribution in normal faulted shallow burial limestones, Malta, and the implications for fluid flow. Journal of Structural Geology, 114, 22-42. https://doi.org/10.1016/j.jsg.2018.05.024
Courgeon, S., Jorry, S. J., Jouet, G., Camoin, G., BouDagher-Fadel, M. K., Bachèlery, P., Caline, B., Révillon, S., Thomas, Y., Thereau, E., Guérin, C., 2017. Impact of tectonic and volcanism on the Neogene evolution of isolated carbonate platforms (SW Indian Ocean). Sedimentary Geology, 355, 114-131. https://doi.org/10.1016/j.sedgeo.2017.04.008
Cruden, A.R., McCaffrey, K.J.W., Bunger, A.P., 2018. Geometric Scaling of Tabular Igneous Intrusions: Implications for Emplacement Laccolith emplacement and Growth Laccolith growth, in: Breitkreuz, C., Rocchi, S. In: Physical Geology of Shallow

Magmatic Systems: Dykes, Sills and Laccoliths, Springer International Publishing. Ed, Advances in Volcanology. Springer International Publishing, Cham. 11–38. https://doi.org/10.1007/11157_2017_1000
DeFelipe, I., Pedreira, D., Pulgar, J.A., Iriarte, E., Mendia, M., 2017. Mantle exhumation and metamorphism in the Basque-Cantabrian Basin (Northern Spain): Stable and clumped isotope analysis in carbonates and comparison with ophicalcites in the North-Pyrenean Zone (Urdach and Lherz): Mantle exhumation in the Basque Cantabrian Basin. Geochemistry, Geophysics, Geosystems 18, 631–652. https://doi.org/10.1002/2016GC006690
Ducoux, M., Jolivet, L., Callot, J. -P., Aubourg, C., Masini, E., Lahfid, A., Homonnay, E., Cagnard, F., Gumiaux, C., Baudin, T., 2019. The Nappe des Marbres Unit of the Basque-Cantabrian Basin: The Tectono-Thermal Evolution of a Fossil Hyperextended Rift Basin. Tectonics 38, 3881–3915. https://doi.org/10.1029/2018TC005348
Ducoux, M., Jolivet, L., Masini, E., Augier, R., Lahfid, A., Bernet, M., Calassou, S., 2021. Distribution and intensity of High-Temperature Low-Pressure metamorphism across the Pyrenean-Cantabrian belt: constraints on the thermal record of the pre-orogenic hyperextension rifting. BSGF - Earth Sciences Bulletin 2021, 192, 43. https://doi.org/10.1051/bsgf/2021029
Durlet, C., Loreau, J.-P., 1996. Sequence diagénétique intrinsèque des surfaces durdes : mise en evidence de surfaces d'imersion et de leur ablation marine. Exemple de la plate-forme bourguignonne, Bajocien (France). Comptes Rendus de l'Académie des Sciences, Series IIA 324, 1001–1008. https://doi.org/10.1016/S1251-8050(97)83985-7
Fernández-Mendiola, P.A.F., García-Mondéjar, J.G., 1983. Estudio geológico del Anticlinorio de Bilbao en el sector del Duranguesado. Kobie 13, 299–324. ISSN 0211-1942
Fernández-Mendiola, P.A.F., 1987. El Complejo Urgoniano en el sector oriental del Anticlinorio de Bilbao. Kobie 16, 7-184. ISSN 0214-6967
Fernández-Mendiola, P.A., García-Mondéjar, J., 1989. Sedimentation of a Lower Cretaceous (Aptian) coral mound complex, Zaraya Mountains, northern Spain. Geological Magazine 126, 423–434. https://doi.org/10.1017/S0016756800006609
Fernández-Mendiola, P.A., García-Mondejar, J., 1990. Mid-cretaceous palaeogeographical evolution of the central Basque-Cantabrian basin (northern Spain). Palaeogeography, Palaeoclimatology, Palaeoecology 81, 115–126. https://doi.org/10.1016/0031-0182(90)90043-7
Fernández-Mendiola, P.A., García-Mondéjar, J., 1991. Depositional history of Aptian-Albian carbonate platforms: Aitzgorri Massif, northern Spain. Cretaceous Research 12, 293–320. https://doi.org/10.1016/0195-6671(91)90038-E
Fernández-Mendiola, P.A., García-Mondéjar, J., 1995. Volcaniclastic sediments in the early Albian Mañaria carbonate platform (northern Spain). Cretaceous Research 16, 451–463. https://doi.org/10.1006/cres.1995.1031
Fernández-Mendiola, P.A., García-Mondéjar, J., 1997. Isolated carbonate platform of Caniego, Spain: A test of the latest Albian worldwide sea-level changes. Geological Society of America Bulletin 109, 176–194. https://doi.org/10.1130/0016-7606(1997)109<0176:ICPOCS>2.3.CO;2
Fernández-Mendiola, P.A., García-Mondéjar, J., 2003. Carbonate platform growth influenced by contemporaneous basaltic intrusion (Albian of Larrano, Spain): Carbonate platform with basalt intrusion. Sedimentology 50, 961–978. https://doi.org/10.1046/j.1365-3091.2003.00591.x
Fernández-Mendiola, P.A., Gómez-Pérez, I., García-Mondéjar, J., 1993. Aptian–Albian Carbonate Platforms Central Basque–Cantabrian Basin, Northern Spain, in: Cretaceous Carbonate Platforms. American Association of Petroleum Geologists Memoir 56, 315-

324. https://doi.org/10.1306/M56578C25
Ferretti, A., Messori, F., Di Bella, M., Sabatino, G., Quartieri, S., Cavalazzi, B., Italiano, F., Barbieri, R., 2019. Armoured sponge spicules from Panarea Island (Italy): Implications for their fossil preservation. Palaeogeography, Palaeoclimatology, Palaeoecology 536, 109379. https://doi.org/10.1016/j.palaeo.2019.109379
Galland, O., Holohan, E., van Wyk de Vries, B., Burchardt, S., 2015. Laboratory Modelling of Volcano Plumbing Systems: A Review. In: Physical Geology of Shallow Magmatic Systems: Dykes, Sills and Laccoliths, Springer International Publishing. Ed, Advances in Volcanology. Springer International Publishing, Cham. 147–214. https://doi.org/10.1007/11157_2015_9
García-Garmilla, F., Carracedo-Sanchez, M., 1989. Diagenetic processes in the Ibarretxe Member (Lower Cretaceous, Bilbao, Northern Spain). Kobie 18, 51–62. ISSN 0214-6967
García-Mondéjar, J., 1990. The Aptian-Albian Carbonate Episode of the Basque-Cantabrian Basin (Northern Spain): General Characteristics, Controls and Evolution. In: Carbonate Platforms: Facies, Sequences and Evolution. Blackwell Publishing. Special Publication of the International Association of Sedimentologists 9, pp. 257–290. https://doi.org/10.1002/9781444303834.ch10
García-Mondéjar, J., 1996. Plate reconstruction of the Bay of Biscay. Geology 24, 635-638. https://doi.org/10.1130/0091-7613(1996)024<0635:PROTBO>2.3.CO;2
García-Mondéjar, J., Agirrezabala, L.M., Aranburu, A., Fernández-Mendiola, P.A., Gómez-Pérez, I., López-Horgue, M., Rosales, I., 1996. Aptian-Albian tectonic pattern of the Basque— Cantabrian Basin (Northern Spain). Geological Journal 31, 13–45. https://doi.org/10.1002/(SICI)1099-1034(199603)31:1<13::AID-GJ689>3.0.CO;2-Y
García-Mondéjar, J., López-Horgue, M. A., Aranburu, A., Fernández- Mendiola, P. A., 2005. Pulsating subsidence during a rift episode: stratigraphic and tectonic consequences (Aptian–Albian, Northern Spain). Terranova, 17, 517–525. https://doi.org/10.1111/j.1365-3121.2005.00644.x
García-Mondéjar, J., Carracedo-Sánchez, M., Owen, H.G., Fernández-Mendiola, P.A., 2018. The Early Aptian volcanic episode of Gutiolo (N Spain): Expression of the Bilbao Rift Fault Zone. Geological Journal 54, 3509–3526. https://doi.org/10.1002/gj.3342
García-Senz, J., Pedrera, A., Ayala, C., Ruiz-Constán, A., Robador, A., Rodríguez-Fernández, L.R., 2020. Inversion of the north Iberian hyperextended margin: the role of exhumed mantle indentation during continental collision. Geological Society, London, Special Publications 490, 177–198. https://doi.org/10.1144/SP490-2019-112
Garrote Ruiz, A., Garcia Portero, J., Munoz Jimerez, L., Arriola Garrido, A., Eguiguren Altuna, E., Garcia Pascual, I., Garrote Ruiz, R., 1990. Mapa Geologico Del Pais Vasco, 1-25.000, Ente Vasco De La Energia publishing.
Georgieva, M.N., Taboada, S., Riesgo, A., Díez-Vives, C., De Leo, F.C., Jeffreys, R.M., Copley, J.T., Little, C.T.S., Ríos, P., Cristobo, J., Hestetun, J.T., Glover, A.G., 2020. Evidence of Vent-Adaptation in Sponges Living at the Periphery of Hydrothermal Vent Environments: Ecological and Evolutionary Implications. Frontiers in Microbiology 11, 1636. https://doi.org/10.3389/fmicb.2020.01636
Girard, J.-P., 1985. Diagenèse hydrothermale tardive des sédiments greso-argileux du protérozoïque supérieur du bassin de Taoudeni (Afrique de l'Ouest). 253p. (Thèse de doctorat). Poitiers, Université de Poitiers. http://www.theses.fr/1985POIT2054
Girard, J.-P., Deynoux, M., Nahon, D., 1989. Diagenesis of the upper Proterozoic siliciclastic sediments of the Taoudeni Basin (West Africa) and relation to diabase emplacement. Journal of Sedimentary Research 59, 233–248. https://doi.org/10.1306/212F8F58-2B24-11D7-8648000102C1865D

Glazner, A.F., Coleman, D.S., Mills, R.D., 2018. The Volcanic-Plutonic Connection. In: Physical Geology of Shallow Magmatic Systems: Dykes, Sills and Laccoliths, Springer International Publishing. Ed, Advances in Volcanology. Springer International Publishing, Cham, 61–82. https://doi.org/10.1007/11157_2015_11

Godeau, N., Deschamps, P., Guihou, A., Leonide, P., Tendil, A., Gerdes, A., Hamelin, B., Girard, J.-P., 2018. U-Pb dating of calcite cement and diagenetic history in microporous carbonate reservoirs: Case of the Urgonian Limestone, France. Geology 46, 247–250. https://doi.org/10.1130/G39905.1

Godet, A., Durlet, C., Spangenberg, J.E., Föllmi, K.B., 2016. Estimating the impact of early diagenesis on isotope records in shallow-marine carbonates: A case study from the Urgonian Platform in western Swiss Jura. Palaeogeography, Palaeoclimatology, Palaeoecology 454, 125–138. https://doi.org/10.1016/j.palaeo.2016.04.029

Gomez-Perez, I., Aranburu Artano, A., Fernández Mendiola, P.Á., García Mondéjar, J., 1994. Un sistema de paleoalto carbonatado-surco siliciclástico (Gorbea-Artzentales, Albiense medio, Bizkaia). Geogaceta 16, 74-77. ISSN: 0213683X

González, F.J., Rincón-Tomás, B., Somoza, L., Santofimia, E., Medialdea, T., Madureira, P., López-Pamo, E., Hein, J.R., Marino, E., de Ignacio, C., Reyes, J., Hoppert, M., Reitner, J., 2020. Low-temperature, shallow-water hydrothermal vent mineralization following the recent submarine eruption of Tagoro volcano (El Hierro, Canary Islands). Marine Geology 430, 106333. https://doi.org/10.1016/j.margeo.2020.106333

Groshong Jr, R. H., 1988. Low-temperature deformation mechanisms and their interpretation. Geological Society of America Bulletin, 100(9), 1329-1360. https://doi-org.insu.bib.cnrs.fr/10.1130/0016-7606(1988)100<1329:LTDMAT>2.3.CO;2

Hacker, D.B., Rowley, P.D., Biek, R.F., 2018. Catastrophic Collapse Features in Volcanic Terrains: Styles and Links to Subvolcanic Magma Systems, In: Physical Geology of Shallow Magmatic Systems: Dykes, Sills and Laccoliths, Springer International Publishing. Ed, Advances in Volcanology. Springer International Publishing, Cham. 215–248. https://doi.org/10.1007/11157_2017_1001

Hall, D. L., Cohen, L. H., Schiffman, P., 1988. Hydrothermal alteration associated with the iron hat iron skarn deposit, eastern Mojave Desert, San Bernardino County, California. Economic Geology 83 (3), 568-587. https://doi.org/10.2113/gsecongeo.83.3.568

Hall-Spencer, J.M., Rodolfo-Metalpa, R., Martin, S., Ransome, E., Fine, M., Turner, S.M., Rowley, S.J., Tedesco, D., Buia, M.-C., 2008. Volcanic carbon dioxide vents show ecosystem effects of ocean acidification. Nature 454, 96–99. https://doi.org/10.1038/nature07051

Horita, J., 2014. Oxygen and carbon isotope fractionation in the system dolomite–water– CO2 to elevated temperatures. Geochimica et Cosmochimica Acta 129, 111–124. https://doi.org/10.1016/j.gca.2013.12.027

Jacquemyn, C., El Desouky, H., Hunt, D., Casini, G., Swennen, R., 2014. Dolomitization of the Latemar platform: Fluid flow and dolomite evolution. Marine and Petroleum Geology 55, 43–67. https://doi.org/10.1016/j.marpetgeo.2014.01.017

Jakubowicz, M., Agirrezabala, L.M., Belka, Z., Siepak, M., Dopieralska, J., 2022. Sr–Nd isotope decoupling at Cretaceous hydrocarbon seeps of the Basque-Cantabrian Basin (Spain): Implications for tracing volcanic-influenced fluids in sedimented rifts. Marine and Petroleum Geology 135, 105340. https://doi.org/10.1016/j.marpetgeo.2021.105430

Jakubowicz, M., Agirrezabala, L.M., Dopieralska, J., Siepak, M., Kaim, A., Belka, Z., 2021. The role of magmatism in hydrocarbon generation in sedimented rifts: A Nd isotope perspective from mid-Cretaceous methane-seep deposits of the Basque-Cantabrian Basin, Spain. Geochimica et Cosmochimica Acta 303, 223–248.

https://doi.org/10.1016/j.gca.2021.03.025
Jakubowicz, M., Dopieralska, J., Belka, Z., 2015. Tracing the composition and origin of fluids at an ancient hydrocarbon seep (Hollard Mound, Middle Devonian, Morocco): A Nd, REE and stable isotope study. Geochimica et Cosmochimica Acta 156, 50–74. https://doi.org/10.1016/j.gca.2015.02.027
Jébrak, M., 1997. Hydrothermal breccias in vein-type ore deposits: A review of mechanisms, morphology and size distribution. Ore Geology Reviews 12, 111–134. https://doi.org/10.1016/S0169-1368(97)00009-7
Kim, S. T., O'Neil, J. R., 1997. Equilibrium and nonequilibrium oxygen isotope effects in synthetic carbonates. Geochimica et cosmochimica acta, 61 (16), 3461-3475. https://doi.org/10.1016/S0016-7037(97)00169-5
Lagabrielle, Y., Labaume, P., de Saint Blanquat, M., 2010. Mantle exhumation, crustal denudation, and gravity tectonics during Cretaceous rifting in the Pyrenean realm (SW Europe): Insights from the geological setting of the lherzolite bodies. Tectonics 29, TC1042. https://doi.org/10.1029/2009TC002588
Léonide, P., Fournier, F., Reijmer, J.J.G., Vonhof, H., Borgomano, J., Dijk, J., Rosenthal, M., van Goethem, M., Cochard, J., Meulenaars, K., 2014. Diagenetic patterns and pore space distribution along a platform to outer-shelf transect (Urgonian limestone, Barremian–Aptian, SE France). Sedimentary Geology 306, 1–23. https://doi.org/10.1016/j.sedgeo.2014.03.001
Lescoutre, R., Manatschal, G., 2020. Role of rift-inheritance and segmentation for orogenic evolution: example from the Pyrenean-Cantabrian system. BSGF - Earth Sciences Bulletin 191, 18. https://doi.org/10.1051/bsgf/2020021
Lin, Y. S., Lui, H. K., Lee, J., Chen, C. T. A., Burr, G. S., Chou, W. C., Kuo, F. W., 2019. Fates of vent CO2 and its impact on carbonate chemistry in the shallow-water hydrothermal field offshore Kueishantao Islet, NE Taiwan. Marine Chemistry, 210, 1-12. https://doi.org/10.1016/j.marchem.2019.02.002
Lokier, S.W., 2021. Marine carbonate sedimentation in volcanic settings. Geological Society, London, Special Publications. In: Volcanic Processes in the Sedimentary Record: When Volcanoes Meet the Environment. Geological Society, London, Special Publications, 520, SP520-2020–251. https://doi.org/10.1144/SP520-2020-251
López-Cilla, I., Rosales, I., Najarro, M., 2012. Diagenesis in Lower Cretaceous platform carbonates of northern Spain (NW Cantabria): an example of multistage dolomitization and calcite cementation. Geofluids 7, Abstract book, Paris, 205–208. https://doi.org/10.1111/gfl.12037
Magee, C., Hunt-Stewart, E., Jackson, C.A.-L., 2013. Volcano growth mechanisms and the role of sub-volcanic intrusions: Insights from 2D seismic reflection data. Earth and Planetary Science Letters 373, 41–53. https://doi.org/10.1016/j.epsl.2013.04.041
Magee, C., Jackson, C. a.-L., Schofield, N., 2014. Diachronous sub-volcanic intrusion along deep-water margins: insights from the Irish Rockall Basin. Basin Research 26, 85–105. https://doi.org/10.1111/bre.12044
Magee, C., Maharaj, S.M., Wrona, T., Jackson, C.A.-L., 2015. Controls on the expression of igneous intrusions in seismic reflection data. Geosphere 11, 1024–1041. https://doi.org/10.1130/GES01150.1
Martin, U., Breitkreuz, C., Egenho, S., Enos, P., Jansa, L., 2004. Shallow-marine phreatomagmatic eruptions through a semi-solidified carbonate platform (ODP Leg 144, Site 878, Early Cretaceous, MIT Guyot, West Pacific). Marine Geology 22, 251-272. https://doi.org/10.1016/S0025-3227(03)00358-X
Mathieu, L., Van Wyk de Vries, B., 2009. Edifice and substrata deformation induced by intrusive complexes and gravitational loading in the Mull volcano (Scotland). Bulletin

of Volcanology 71, 1133–1148. https://doi.org/10.1007/s00445-009-0295-5
Mendia, M.S., Ibarguchi, J.I.G., 1991. High-grade metamorphic rocks and peridotites along the Leiza Fault (Western Pyrenees, Spain). Geologische Rundschau 80, 93–107. https://doi.org/10.1007/BF01828769
Millán, M.I., Weissert, H.J., López-Horgue, M.A., 2014. Expression of the late Aptian cold snaps and the OAE1b in a highly subsiding carbonate platform (Aralar, northern Spain). Palaeogeography, Palaeoclimatology, Palaeoecology 411, 167–179. https://doi.org/10.1016/j.palaeo.2014.06.024
Molina, J.M., Vera, J.A., 2000. Influencia del subvolcanismo en la sedimentación pelágica del Jurásico medio (Sierra de San Pedro, provincia de Jaén, Subbético medio). Geogaceta 27, 111–114. ISSN: 0213683X
Moller Hansen, D., Cartwright, J.A., 2006. Saucer-shaped sill with lobate morphology revealed by 3D seismic data: Implications for resolving a shallow-level sill emplacement mechanism. Journal of The Geological Society 163, 509–523. https://doi.org/10.1144/0016-764905-073
Montigny, R., Azambre, B., Rossy, M., Thuizat, R., 1986. K-Ar study of cretaceous magmatism and metamorphism in the Pyrenees: Age and length of rotation of the Iberian Peninsula. Tectonophysics 129, 257–273. https://doi.org/10.1016/0040-1951(86)90255-6
Moore, C.H., 2001. Carbonate Reservoirs: Porosity Evolution and Diagenesis in Sequence Stratigraphic Framework: By Clyde Moore, Published by Elsevier, Amsterdam, Developments in Sedimentology 55 - 1st Edition, 444. ISBN: 9780444508386
Morgan, S., Stanik, A., Horsman, E., Tikoff, B., de Saint Blanquat, M., Habert, G., 2008. Emplacement of multiple magma sheets and wall rock deformation: Trachyte Mesa intrusion, Henry Mountains, Utah. Journal of Structural Geology 30, 491–512. https://doi.org/10.1016/j.jsg.2008.01.005
Motte, G., Hoareau, G., Callot, J.-P., Révillon, S., Piccoli, F., Calassou, S., Gaucher, E.C., 2021. Rift and salt-related multi-phase dolomitization: example from the northwestern Pyrenees. Marine and Petroleum Geology 126, 104932. https://doi.org/10.1016/j.marpetgeo.2021.104932
Mounji, D., Bourque, P.-A., Savard, M.M., 1998. Hydrothermal origin of Devonian conical mounds (kess-kess) of Hamar Lakhdad Ridge, Anti-Atlas, Morocco. Geology 26, 1123-1126. https://doi.org/10.1130/0091-7613(1998)026<1123:HOODCM>2.3.CO;2
Nader, F.H., López-Horgue, M.A., Shah, M.M., Dewit, J., Garcia, D., Swennen, R., Iriarte, E., Muchez, P., Caline, B., 2012. The Ranero Hydrothermal Dolomites (Albian, Karrantza Valley, Northwest Spain): Implications on Conceptual Dolomite Models. Oil & Gas Sciences and Technology – Review from IFP Energies nouvelles 67, 9–29. https://doi.org/10.2516/ogst/2011165
Nehlig, P., Lacquement, F., Bernard, J., Caroff, M., Deparis, J., Jaouen, T., Pelleter, A.-A., Perrin, J., Progon, C., Vittecoq, B., 2013. Notice de la carte géologique de Mayotte. 135p. ISBN: 978-2-7159-2179-5
Neuweiler, F., 1993. Development of albian microbialites and microbialite reefs at marginal platform areas of the Vasco-Cantabrian Basin (Soba reef area, Cantabria, N. Spain). Facies 29, 231–249. https://doi.org/10.1007/BF02536930
Neuweiler, F., Gautret, P., Thiel, V., Lange, R., Michaelis, W., Reitner, J., 1999. Petrology of Lower Cretaceous carbonate mud mounds (Albian, N. Spain): insights into organomineralic deposits of the geological record. Sedimentology 46, 837–859. https://doi.org/10.1046/j.1365-3091.1999.00255.x
Pascal, A., 1985. Les systèmes biosédimentaires urgoniens (Aptien-Albien) sur la marge nord-ibérique. (Mémoire Géologique de l'Université de Dijon), 636p. ISSN : 022-7412
Pascal, A., Przybyla, A., 1989. Processus biosédimentaires et diagénétiques précoces dans les

mud-mounds (Thrombolite-mounds) urgoniens d'Espagne du Nord (Aptien-Albien) et leur signification. Géologie Méditerranéenne 16, 171–183. https://doi.org/10.3406/geolm.1989.1424

Pascault, O., Durlet, C., Saucède, T., Virgone, A., 2022. Geomorphologic and eogenetic impact of CO_2-volcanic seeps into Mayotte lagoon (Comoros Archipelago, Mozambique Channel). 18ième Congrès Français de Sédimentologie. Sciencesconf.org:asf-brest-2022:419178

Pearson, P.N., Ditchfield, P.W., Singano, J., Harcourt-Brown, K.G., Nicholas, C.J., Olsson, R.K., Shackleton, N.J., Hall, M.A., 2001. Warm tropical sea surface temperatures in the Late Cretaceous and Eocene epochs. Nature 413, 481–487. https://doi.org/10.1038/35097000

Pedrera, A., García-Senz, J., Ayala, C., Ruiz-Constán, A., Rodríguez-Fernández, L.R., Robador, A., González Menéndez, L., 2017. Reconstruction of the Exhumed Mantle Across the North Iberian Margin by Crustal-Scale 3-D Gravity Inversion and Geological Cross Section: Mantle Along the Basque-Cantabrian Basin. Tectonics 36, 3155–3177. https://doi.org/10.1002/2017TC004716

Pedrera, A., García-Senz, J., Peropadre, C., Robador, A., López-Mir, B., Díaz-Alvarado, J., Rodríguez-Fernández, L.R., 2021. The Getxo crustal-scale cross-section: Testing tectonic models in the Bay of Biscay-Pyrenean rift system. Earth-Science Reviews 212, 103429. https://doi.org/10.1016/j.earscirev.2020.103429

Planke, S., Rasmussen, T., Rey, S.S., Myklebust, R., 2005. Seismic characteristics and distribution of volcanic intrusions and hydrothermal vent complexes in the Vøring and Møre basins. Petroleum Geology Conference series 6, 833–844. https://doi.org/10.1144/0060833

Planke, S., Svensen, H., Myklebust, R., Bannister, S., Manton, B., Lorenz, L., 2018. Geophysics and Remote Sensing, In: Physical Geology of Shallow Magmatic Systems: Dykes, Sills and Laccoliths, Springer International Publishing. Ed, Advances in Volcanology. Springer International Publishing, Cham, 131–146. https://doi.org/10.1007/11157_2014_6

Polteau, S., Mazzini, A., Galland, O., Planke, S., Malthe-Sørenssen, A., 2008. Saucer-shaped intrusions: Occurrences, emplacement and implications. Earth and Planetary Science Letters 266, 195–204. https://doi.org/10.1016/j.epsl.2007.11.015

Prokoph, A., Shields, G.A., Veizer, J., 2008. Compilation and time-series analysis of a marine carbonate $\delta^{18}O$, $\delta^{13}C$, $^{87}Sr/^{86}Sr$ and $\delta^{34}S$ database through Earth history. Earth-Science Reviews 87, 113–133. https://doi.org/10.1016/j.earscirev.2007.12.003

Pucéat, E., Lécuyer, C., Sheppard, S.M.F., Dromart, G., Reboulet, S., Grandjean, P., 2003. Thermal evolution of Cretaceous Tethyan marine waters inferred from oxygen isotope composition of fish tooth enamels. Paleoceanography 18, 02, 1029. https://doi.org/10.1029/2002PA000823

Quintà, A., Tavani, S., Roca, E., 2012. Fracture pattern analysis as a tool for constraining the interaction between regional and diapir-related stress fields: Poza de la Sal Diapir (Basque Pyrenees, Spain). Geological Society, London, Special Publications 363, 521–532. https://doi.org/10.1144/SP363.25

Rat, P., 1959. Les Pays crétacés Basco-Cantabriques (Espagne). Publication de l'université de Dijon, 18, 525p. (Thèse de doctorat). ISSN 0223-3762

Robador, A., Garcia de Cortazar, A., 1986. Despositos vulcanosedimentarios en el Aptiense-Albiense de la Cuenca Vasco-Cantabrica y su relacion con fracturas de actuacion sinsedimentaria. Spanish Sedimentological Congress 149.

Roberts, N.M., Rasbury, E.T., Parrish, R.R., Smith, C.J., Horstwood, M.S., Condon, D.J., 2017. A calcite reference material for LA-ICP-MS U-Pb geochronology. Geochemistry,

Geophysics, Geosystems 18, 2807–2814. https://doi.org/10.1002/2016GC006784
Roca, E., Ferrer, O., Rowan, M.G., Munoz, J.A., Butille, M., Giles, K.A., Arbues, P., de Matteis, M., 2021. Salt tectonics and controls on halokinetic-sequence development of an exposed deepwater diapir: The Bakio Diapir, Basque-Cantabrian Basin, Pyrenees. Marine and Petroleum Geology 123, 104770. https://doi.org/10.1016/j.marpetgeo.2020.104770
Roca, E., Muñoz, J.A., Ferrer, O., Ellouz, N., 2011. The role of the Bay of Biscay Mesozoic extensional structure in the configuration of the Pyrenean orogen: Constraints from the MARCONI deep seismic reflection survey. Tectonics 30, TC2001. https://doi.org/10.1029/2010TC002735
Rossy, M., 1988. Contribution à l'étude du magmatisme mésozoique du domaine pyrénéen : I, le Trias dans l'ensemble du domaine, II le Crétacé dans les provinces basques d'Espagne (Thèse d'Etat, Université de Besançon). 351p. Order 225.
Rui, G., Gongcheng, Z., Jinwei, Z., Xingbin, Z., Junbang, L., Dawei, Y., Shuang, S., 2013. Fingered Intrusion of Shallow Saucer-shaped Igneous Sills: Insights from the Jiaojiang Sag, East China Sea. Acta Geologica Sinica - English Edition 87, 1306–1318. https://doi.org/10.1111/1755-6724.12130
Schlagintweit, F., Bover-Arnal, T., 2013. Remarks on Bačinella Radoičić, 1959 (type species B. irregularis) and its representatives. Facies 59, 59–73. https://doi.org/10.1007/s10347-012-0309-1
Schlagintweit, F., Bover-Arnal, T., Salas, R., 2010. New insights into Lithocodium aggregatum Elliott 1956 and Bacinella irregularis Radoičić 1959 (Late Jurassic–Lower Cretaceous): two ulvophycean green algae (? Order Ulotrichales) with a heteromorphic life cycle (epilithic/euendolithic). Facies 56, 509-547. https://doi.org/10.1007/s10347-010-0222-4
Senger, K., Buckley, S.J., Chevallier, L., Fagereng, Å., Galland, O., Kurz, T.H., Ogata, K., Planke, S., Tveranger, J., 2015. Fracturing of doleritic intrusions and associated contact zones: Implications for fluid flow in volcanic basins. Journal of African Earth Sciences 102, 70–85. https://doi.org/10.1016/j.jafrearsci.2014.10.019
Shah, M.M., Afridi, S., Khan, E.U., Rahim, H.U., Mustafa, M.R., 2021. Diagenetic Modifications and Reservoir Heterogeneity Associated with Magmatic Intrusions in the Devonian Khyber Limestone, Peshawar Basin, NW Pakistan. Geofluids 2021, 18. https://doi.org/10.1155/2021/8816465
Sibley, D. F., Gregg, J. M., 1987. Classification of dolomite rock textures. Journal of sedimentary Research, 57(6), 967-975. https://doi.org/10.1306/212F8CBA-2B24-11D7-8648000102C1865D
Svensen, H.H., Planke, S., Neumann, E.-R., Aarnes, I., Marsh, J.S., Polteau, S., Harstad, C.H., Chevallier, L., 2018. Sub-Volcanic Intrusions and the Link to Global Climatic and Environmental Changes, in: Physical Geology of Shallow Magmatic Systems: Dykes, Sills and Laccoliths, Springer International Publishing. Ed, Advances in Volcanology. Springer International Publishing, Cham, 249–272. https://doi.org/10.1007/11157_2015_10
Svensen, H.H., Planke, S., Neumann, E.-R., Aarnes, I., Marsh, J.S., Polteau, S., Harstad, C.H., Chevallier, L., 2015. Sub-Volcanic Intrusions and the Link to Global Climatic and Environmental Changes, in: Physical Geology of Shallow Magmatic Systems: Dykes, Sills and Laccoliths, Springer International Publishing. Ed, Advances in Volcanology. Springer International Publishing, Cham, 249–272. https://doi.org/10.1007/11157_2015_10
Sydnes, M., Fjeldskaar, W., Grunnaleite, I., Løtveit, I.F., Mjelde, R., 2019. The Influence of Magmatic Intrusions on Diagenetic Processes and Stress Accumulation. Geosciences 9,

477. https://doi.org/10.3390/geosciences9110477
Tang, X.Y., Gong-Cheng, Z., Jian-She, L., Shu-Chun, Y., Song, R., Sheng-Biao, H,U., 2014. Modelling of thermal effects of igneous intrusions on the temperature field and organic maturity in the Changchang Sag, Qiongdongnan Basin, South China Sea. Chinese Journal of Geophysics, 57 (2), 219-229. https://doi.org/10.1002/cjg2.20098
Tugend, J., Manatschal, G., Kusznir, N.J., Masini, E., Mohn, G., Thinon, I., 2014. Formation and deformation of hyperextended rift systems: Insights from rift domain mapping in the Bay of Biscay-Pyrenees. Tectonics 33, 1239–1276. https://doi.org/10.1002/2014TC003529
Ubide, T., Wijbrans, J.R., Galé, C., Arranz, E., Lago, M., Larrea, P., 2014. Age of the Cretaceous alkaline magmatism in northeast Iberia: Implications for the Alpine cycle in the Pyrenees. Tectonics 33, 1444–1460. https://doi.org/10.1002/2013TC003511
Westerman, D., Rocchi, S., Breitkreuz, C., Stevenson, C., Wilson, P., 2018. Structures Related to the Emplacement of Shallow-Level Intrusions, in: Physical Geology of Shallow Magmatic Systems: Dykes, Sills and Laccoliths, Springer International Publishing. Ed, Advances in Volcanology. Springer International Publishing, Cham, 83–118. https://doi.org/10.1007/11157_2017_31
Wiese, F., Kiel, S., Pack, A., Walliser, E.O., Agirrezabala, L.M., 2015. The beast burrowed, the fluid followed – Crustacean burrows as methane conduits. Marine and Petroleum Geology, Carbonate conduits linked to hydrocarbon-enriched fluid escape 66, 631–640. https://doi.org/10.1016/j.marpetgeo.2015.03.004
Woodhead, J.D., Hergt, J.M., 2001. Strontium, neodymium and lead isotope analyses of NIST glass certified reference materials: SRM 610, 612, 614. Geostandards Newsletter 25, 261–266. https://doi.org/10.1111/j.1751-908X.2001.tb00601.x
Zinke, J., Reijmer, J.J.G., Thomassin, B.A., 2001. Seismic architecture and sediment distribution within the Holocene barrier reef–lagoon complex of Mayotte (Comoro archipelago, SW Indian Ocean). Palaeogeography, Palaeoclimatology, Palaeoecology 175, 343–368. https://doi.org/10.1016/S0031-0182(01)00379-0
Zinke, J., Reijmer, J.J.G., Thomassin, B.A., Dullo, W.-C., Grootes, P.M., Erlenkeuser, H., 2003. Postglacial flooding history of Mayotte Lagoon (Comoro Archipelago, southwest Indian Ocean). Marine Geology 194, 181–196. https://doi.org/10.1016/S0025-3227(02)00705-3